UNIVERSITÀ DI PISA

TESI DI LAUREA MAGISTRALE

# Nonequilibrium Steady-State Analysis of a Boundary-Driven Interacting Quantum Spin Chain


*Candidata:*
Francesca COLLU

*Relatore:*
Dr. Davide ROSSINI

Facoltà di Scienze
Corso di Laurea Magistrale in Fisica


Anno Accademico 2018/2019

# Contents

# Introduction

Open quantum systems are physical systems coupled with an environment with which they exchange information. Studying the dynamics of open systems is not an easy problem, due to the complexity of the interaction between the parts involved. In order to overcome this difficulty, over the decades several analytical e numerical methods have been developed. In addition to these more "traditional" approaches, over the last decades have been investigated and advanced the field of quantum simulators: experimental platforms that reproduce Hamiltonian models analyzable with difficulty. Their advantage is the fact that the quantum simulators are quantum systems that can be insulated from the environment or with parameters easily tunable in order to replicate the model under consideration.

In order to examine in depth systems that may be simulated, numerical strategies has been used and developed. In the present thesis, we examine three of the most employed numerical methods in the field of strongly correlated quantum systems: the corner-space renormalization method, the quantum trajectories method and the matrix product operators method. We have used these approach to study a XYZ Heisenberg spin-1/2 chain coupled to a pair of dissipators acting only on the edge of the system.

This thesis is organized as follows.

In the first chapter we run the basic concepts of the theory of open systems, introducing the notion of pure and mixed states and the density matrix formalism. In particular, we talk about dynamics of open systems, described by a master equation derived under the condition of having a Markovian evolution for the system. In the end of the chapter, technical concepts concerning quantum systems are introduced.

In chapter 2, we go through the most recent development in the field of quantum simulator concluding with some example of experimental platform that simulate spin systems.

Chapter 3 deals with numerical approaches in solving open many-body system problems, with a detailed report about the three numerical methods used in the present work.

Chapter 4 and chapter 5 contain the original part of the work; after a description of the model under study, some observables are analyzed: magnetization profile, two-point correlation function and spin current. In the last section, an investigation on the presence of a phase transition is performed.

# Chapter 1

# Open Quantum Systems

> The motivation for studying open systems is that all realistic systems are open.
>
> *John Preskill*

The world we live in is constituted by parts that communicate with each other and exchange information. The difficulty of describing it, lies in the complexity of the interactions between those parts. To overcome this problem, simplifications and easier mathematical representations have been developed: in the following we will see some of them.

This chapter has the purpose of giving a recap of the most useful characteristics of open quantum systems, in the perspective of studying an open many-body system and, as stated before, a 1D spin chain, in particular. First of all, in section 1.1 we will specify the difference between closed and open systems and we will derive the density matrix formalism; then, in section 1.2 we will gather the master equation useful for describing the dynamics of open quantum systems; finally, in section 1.3 we will see some important technical concept that we will use effectively in the original part of the present work.

## 1.1 Mathematical Backgroud

Before we explore the field of open quantum systems, we now assess the basic differences between a closed and an open quantum system are and why different approaches are required to treat these two distinct kinds of systems. First of all, let us define a *closed* system as a physical system which does not exchange any information with its surroundings. On the contrary, an *open* system is a physical system that interacts with the environment in which it is.

In this section, we will briefly look at the different approaches in the study of the dynamics in closed and open quantum systems.

### 1.1.1 Pure and mixed states: the density matrix formalism

First of all, it is useful to consider another formalism in addition to that used normally for handling pure states, i.e. states that can be described by a single wave function. We now introduce the *density matrix* formalism for managing the so-called mixed states, although - as we will see - it can be used also for pure states [5].

Quantum systems prepared in such a way that their state vector being obtained performing a *maximal measurement*, in the sense that the maximum possible information has been acquired (all values of a complete set of commuting observables have been ascertained), are in a pure state.

Quantum systems for which the maximum possible information is not available, are said to be in mixed state and are called *statistical mixtures*.

Let us consider a system consisting of an ensemble of N sub-systems $\alpha = 1, 2, \ldots, N$. We suppose that every sub-system is in a pure state $|\psi_\alpha\rangle$. Then, we choose a complete set of basis vectors $|n\rangle$, such that $\sum_n |n\rangle \langle n| = \mathbb{1}$. Let us expand the pure states in the basis $\{|n\rangle\}$:

$$|\psi_\alpha\rangle = \sum_n c_n^{(\alpha)} |n\rangle ,$$

where the coefficients $c_n^{(\alpha)}$ are such that

$$\sum_n |c_n^{(\alpha)}|^2 = 1.$$

Now let us consider an observable represented by an operator $A$; its expectation value in the pure state $\psi_\alpha$ is:

$$\begin{aligned} \langle A \rangle_\alpha &= \langle \psi_\alpha | A | \psi_\alpha \rangle && (1.1)\\ &= \sum_n \sum_{n'} c_n^{(\alpha)} c_{n'}^{(\alpha)*} \langle n' | A | n \rangle && (1.2)\\ &= \sum_n \sum_{n'} \langle n | \psi_\alpha \rangle \langle \psi_\alpha | n' \rangle \langle n' | A | n \rangle . && (1.3) \end{aligned}$$

The average value of A over the ensemble is

$$\langle A \rangle = \sum_{\alpha=1}^{N} w_\alpha \langle A \rangle_\alpha, \tag{1.4}$$

where the coefficients $w_\alpha$ are the statistical weight of the pure states $|\psi_\alpha\rangle$, i.e. the probability of finding the system in this state. So the $w_\alpha$ are such that

$$0 \leq w_\alpha \leq 1 \tag{1.5}$$

and

$$\sum_{\alpha=1}^{N} w_\alpha = 1.$$

Using the result 1.2 in the 1.4, we obtain:

$$\begin{aligned} \langle A \rangle &= \sum_{\alpha=1}^{N} \sum_n \sum_{n'} w_\alpha c_{n'}^{(\alpha)*} c_n^{(\alpha)} \langle n' | A | n \rangle && (1.6)\\ &= \sum_{\alpha=1}^{N} \sum_n \sum_{n'} \langle n | \psi_\alpha \rangle w_\alpha \langle \psi_\alpha | n' \rangle \langle n' | A | n \rangle . && (1.7) \end{aligned}$$

We now introduce the *density operator*

$$\rho = \sum_{\alpha=1}^{N} |\psi_\alpha\rangle w_\alpha \langle \psi_\alpha| , \tag{1.8}$$

whose representation in the basis $\{n\}$ gives us the density matrix:

$$\rho_{nn'} = \langle n| \rho |n'\rangle = \sum_{\alpha=1}^{N} w_\alpha c_{n'}^{(\alpha)*} c_n^{(\alpha)}. \tag{1.9}$$

So, returning to the 1.7 in the definition of the density matrix, we observe that:

$$\langle A\rangle = \sum_n \sum_{n'} \langle n| \rho |n'\rangle \langle n'| A |n\rangle = \mathrm{Tr}(\rho A).$$

It is worth stressing the fact that the knowledge of the density matrix enables us to obtain the ensemble average of A.

Anyway, this leads us to the first of the three fundamental characteristics of the density matrix, that is:

$$\mathrm{Tr}(\rho) = 1, \tag{1.10}$$

that is true if we make the assumption that the $|\psi_\alpha\rangle$ are normalized to unity. If they are not, then the ensemble average of A is given by

$$\langle A\rangle = \frac{\mathrm{Tr}(\rho A)}{\mathrm{Tr}(\rho)}. \tag{1.11}$$

The second characteristic of the density matrix is that it is Hermitian, namely:

$$\langle n| \rho |n'\rangle = \langle n'| \rho |n\rangle^* . \tag{1.12}$$

The third characteristic arises from the observation of the diagonal elements of $\rho$:

$$\rho_{nn} = \langle n| \rho |n\rangle = \sum_{\alpha=1}^{N} w_\alpha |c_n^{(\alpha)}|^2, \tag{1.13}$$

which tells us, with the 1.5, that

$$\rho_{nn} \geq 0, \tag{1.14}$$

i.e. $\rho$ is a positive semi-definite matrix. It is worth stress the physical interpretation of the diagonal elements; $w_\alpha$ is the probability of finding the system in the pure state $\psi_\alpha$, while $|c_n^{(\alpha)}|^2$ is the probability of finding $\psi_\alpha$ in the state $|n\rangle$. So, $\rho_{nn}$ gives the probability of finding a member of the ensemble in the state $|n\rangle$.

### 1.1.2 Closed Quantum Systems

Quantum mechanics establishes that the time evolution of a state vector $|\psi(t)\rangle$ is predicted by the Schrödinger equation:

$$i\frac{d}{dt} |\psi(t)\rangle = H(t) |\psi(t)\rangle , \tag{1.15}$$

where $H(t)$ is the Hamiltonian of the closed system; from now on, the Planck's constant $\hbar$ is set equal to 1. The solution of this equation can be written in terms of the unitary time-evolution operator $U(t, t_0)$:

$$|\psi(t)\rangle = U(t, t_0) |\psi(t_0)\rangle , \tag{1.16}$$

where $t_0 < t$. If we substitute the equation 1.16 into the 1.15, we obtain:

$$i\frac{d}{dt}U(t,t_0) = H(t)U(t,t_0), \tag{1.17}$$

subject to the initial condition

$$U(t_0,t_0) = \mathbb{1}. \tag{1.18}$$

We can write the dynamics of a closed system using the density matrix formalism seen in the previous section. In order to do this, let us assume that at a initial time $t_0$ the state of the system is characterized by the density matrix

$$\rho(t_0) = \sum_{\alpha=1}^{N} w_\alpha \left|\psi_\alpha(t_0)\right\rangle \left\langle\psi_\alpha(t_0)\right|,$$

that at a time $t$ evolves in this way:

$$\rho(t) = \sum_{\alpha=1}^{N} w_\alpha U(t,t_0) \left|\psi_\alpha(t_0)\right\rangle \left\langle\psi_\alpha(t_0)\right| U(t,t_0)^\dagger,$$

that is

$$\rho(t) = U(t,t_0)\rho(t_0)U(t,t_0)^\dagger.$$

Differentiating with respect to time the last equation we have

$$\frac{d}{dt}\rho(t) = -i[H(t),\rho(t)] \tag{1.19}$$

i.e. an equation of motion for the density matrix, often called the *Liouville-von Neumann equation* [6].

### 1.1.3 Open Quantum Systems

Now we can go into a more specific definition of open quantum systems. It can be defined as a system $S$ coupled with another quantum system $E$, called the *environment*. Usually, the total system $S + E$ is treated as a closed system, so it follows Hamiltonian dynamics. The interactions between the two sub-systems induce an evolution in the state of the open system $S$, which can no longer be represented by unitary, Hamiltonian dynamics. Following the definitions given in [6], an environment with an infinite number of degrees of freedom such that the frequencies of the modes form a continuum, is called *reservoir*. Also, a reservoir in a thermal equilibrium state is called *bath*.

$|\psi\rangle$

Since $S$ and $E$ are in thermal contact, energy can be exchanged between them; however the interaction is supposed to be weak, so that both $S$ and $E$ at any time can be considered to be in definite energy eigenstates with energies $E_S$ and $E_E$ respectively. Naming $E$ one of the eigenenergies of the combined system, for the conservation of energy we have:

$$E = E_S + E_E.$$

Let $d\Gamma(E)$ be the total number of distinct states of the combined system with energies in the range $[E, E + dE]$. So, the probability the probability of finding the combined

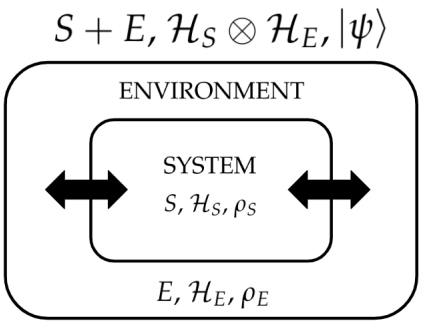


FIGURE 1.1: Schematic representation of an open quantum system.

system with an energy in this range will be[1]:

$$dP = Cd\Gamma(E), \quad E_0 \leq E \leq E_0 + \Delta \tag{1.20}$$

and zero otherwise; C is a constant.

If we call $d\Gamma_S$ and $d\Gamma_E$ the number of states for the system and the environment, respectively, we have:

$$d\Gamma = d\Gamma_S d\Gamma_E, \tag{1.21}$$

so that:

$$dP = Cd\Gamma_S(E_S)d\Gamma_E(E_E)\delta(E - E_S - E_E), \tag{1.22}$$

where the delta function expresses the conservation of energy.

The probability $dP_n$ that the combined system is in a state such that the system S has an energy $E_S$, without regard to the state of the reservoir, can be obtained integrating over the states of the reservoir:

$$\begin{aligned} dP_n &= Cd\Gamma_S(E_n) \int \delta(E - E_n - E_E)d\Gamma_E(E_E) \\ &= Cd\Gamma_S(E_n)\Delta\Gamma_E(E - E_n), \end{aligned} \tag{1.23}$$

where $\Delta\Gamma_E(E - E_n)$ is the total number of states of the environment, that can be written in terms of the entropy $S_E$ of the reservoir:

$$\Delta\Gamma_E = \exp(S_E/k).$$

Since $E_n \ll E$, we can write:

$$S_E(E_E) = S_E(E - E_n) \simeq S_E(E) - \frac{\partial S_E(E)}{\partial E}E_n = S_E(E) - \frac{E_n}{T},$$

where the temperature $T$ has been defined as:

$$\frac{1}{T} = \frac{\partial S}{\partial E}.$$

Substituting in eq. 1.23, we find that

$$dP_n = A\exp(-E_n/kT)d\Gamma_S(E_n), \tag{1.24}$$

[1]This is true because of the postulate of equal *a priori* probabilities, since the combined system is supposed to be close, so it is well described by a micro-canonical ensemble.

where $A$ is defined as

$$A = C \exp\left(S_E(E)/k\right). \tag{1.25}$$

The probability 1.24 can be written in terms of the density matrix, in this way:

$$\rho_{nm} = A \exp\left(-E_n/kT\right)\delta_{nm}.$$

Using the normalization condition $\mathrm{Tr}(\rho) = 1$, we can find $A^{-1} \equiv Q_S$:

$$Q_S(T) = \sum_n \exp\left(-E_n/kT\right) = \mathrm{Tr}[\exp\left(-\beta H_S\right)],$$

where

$$\beta = \frac{1}{kT}$$

$H_S$ is the Hamiltonian of the system $S$ and $Q_S$ is the *partition function*.

So, we can write the density operator in the *canonical ensemble* as:

$$\rho = \frac{1}{Q_S(T)} \exp\left(-\beta H_S\right). \tag{1.26}$$

The average value of an observable O over the ensemble is

$$\begin{aligned} \langle O \rangle = \mathrm{Tr}(\rho O) &= \frac{1}{Q_S} \mathrm{Tr}[\exp\left(-\beta H_S\right) O] \\ &= \frac{\mathrm{Tr}[\exp\left(-\beta H_S\right) O]}{\mathrm{Tr}[\exp\left(-\beta H_S\right)]}. \end{aligned} \tag{1.27}$$

Let us call $\mathcal{H}_S$ and $\mathcal{H}_E$ the Hilbert spaces of the system and the environment, respectively. The Hilbert space of the combined system is given by the tensor product $\mathcal{H}_{S+E} = \mathcal{H}_S \otimes \mathcal{H}_E$. So, the total Hamiltonian can be written in this way:

$$H(t) = H_S \otimes \mathbb{1}_E + \mathbb{1}_S \otimes H_E + H_I(t), \tag{1.28}$$

where $H_S$ and $H_E$ are the free Hamiltonians of the system and the environment, respectively, and $H_I(t)$ is the Hamiltonian describing the interactions between $S$ and $E$.

At this point, we must find a relation between the density matrix $\rho \in \mathcal{H}_{S+E}$ and $\rho_S \in \mathcal{H}_S$; it is given by the partial trace over the environment $B$[2]:

$$\rho_S = \mathrm{Tr}_E(\rho). \tag{1.29}$$

This helps us in the study of the dynamics of the so-called *reduced* density matrix $\rho_S$. Indeed, we can write:

$$\rho_S(t) = \mathrm{Tr}_E[\rho(t)]; \tag{1.30}$$

observing that we assumed the total system to be *closed*, it evolves unitarily so we have:

$$\rho_S(t) = \mathrm{Tr}_B\{U(t, t_0)\rho(t_0)U(t, t_0)^\dagger\}, \tag{1.31}$$

where $U(t, t_0)$ is the time-evolution operator of the combined system $S + E$. So we can use the equation of motion 1.19 and trace over the degrees of freedom of the

[2] A proof of this statement is given, e.g., in [34].

environment, in order to obtain the equation of motion for the $\rho_S(t)$:

$$\frac{d}{dt}\rho_S(t) = -i\,\mathrm{Tr}_B[H(t), \rho(t)]. \tag{1.32}$$

## 1.2 Approximate Description of Open Quantum Systems

If one consider a many-particles system, where the Hilbert space becomes "large", solving exactly the equation 1.32 is rather difficult, because of the fact that the environment may represent a reservoir consisting of infinitely many degrees of freedom, or its modes may be neither known nor controllable, for example. The following will derive a simpler description of the dynamics of an open quantum system.

### 1.2.1 Quantum Dynamical Semigroups

For reasons that will be clear later, let us rewrite the equation 1.32 as a *dynamical map* acting on $\mathcal{H}_S$ that connect the states of the system $S$ from time $t_0$ to time $t_1$, that is:

$$\varepsilon_{(t_1,t_0)}: \quad \rho_S(t_0) \mapsto \rho_S(t_1). \tag{1.33}$$

In order to obtain the way in which this map acts on the states, we consider a system consisting in two sub-systems $S + E$, that are uncorrelated[3] at the initial time $t = 0$, so that

$$\rho(0) = \rho_S(0) \otimes \rho_E(0), \tag{1.34}$$

where $\rho_S(0)$ is the initial state of the system $S$ and $\rho_E(0)$ represents the state of the environment at time $t = 0$. The evolution of the system $S$ from the time $t = 0$ to the time $t > 0$ is governed by the map, in this way:

$$\rho_S(0) \mapsto \rho_S(t) = \varepsilon(t)\rho_S(0) \equiv \mathrm{Tr}_E\{U(t,0)[\rho_S(0) \otimes \rho_E(0)]U^\dagger(t,0)\}. \tag{1.35}$$

Using the spectral decomposition of the density matrix $\rho_E$ of the environment

$$\rho_E = \sum_i \lambda_i \left|\psi_i\right\rangle \left\langle\psi_i\right|,$$

we can perform the partial trace of 1.35 in this basis, obtaining:

$$\begin{aligned} \rho_S(t) &= \sum_{ij} \lambda_i \left\langle\psi_j\right| U(t,0) \left|\psi_i\right\rangle \rho_S(0) \left\langle\psi_i\right| U^\dagger(t,0) \left|\psi_j\right\rangle \\ &= \sum_a M_a \rho_S(0) M_a^\dagger. \end{aligned} \tag{1.36}$$

So, the dynamical map can be expressed in terms of the following so-called *operator-sum* representation:

$$\varepsilon(\rho) = \sum_a M_a \rho M_a^\dagger, \tag{1.37}$$

where the $\{M_a\}$ obey the completeness relation

$$\sum_a M_a^\dagger M_a = \mathbb{1} \tag{1.38}$$

[3] Initial correlations between environment and the open system play significant role in the dynamics of open systems [42].

and are called *Kraus operators* and are defined as

$$M_a = \sqrt{\lambda_i} \langle \psi_j | U(t,0) | \psi_i \rangle_a . \tag{1.39}$$

This object has some essential features that give it the name *completely positive trace-preserving map* or *CPTP map*; as its name suggests, its properties[4] are:

- linearity:
$$\varepsilon(\alpha\rho_1 + \beta\rho_2) = \alpha\varepsilon(\rho_1) + \beta\varepsilon(\rho_2);$$
- preserves Hermiticity:
$$\rho = \rho^\dagger \implies \varepsilon(\rho) = \varepsilon^\dagger(\rho);$$
- preserves positivity[5]:
$$\rho \geq 0 \implies \varepsilon(\rho) \geq 0;$$
- preserves trace:
$$\mathrm{Tr}[\varepsilon(\rho)] = \mathrm{Tr}(\rho).$$

The TPCP maps are called by other names; one of them is *super-operator*, due to its function of connecting operators with operators, rather than vectors with vectors. Another name used in the field of Quantum Information is *quantum channel*, that originates from communication theory and gives the image of the "channel" throughout the state $\rho$ travels to reach its destination as $\varepsilon(\rho)$.

There is a reason why we can say that the TPCP maps form a *dynamical semigroup*: that is because the associative property is satisfied. Indeed, if $\varepsilon_1$ is a TPCP map with $N$ Kraus operators $\{A_a\}$ and $\varepsilon_2$ is a TPCP map with $M$ Kraus operators $\{B_b\}$, than $\varepsilon_1 \circ \varepsilon_2$ has an operator-sum representation with $NM$ Kraus operators $\{A_a B_b\}$.

### 1.2.2 The Markovian Evolution

With a view to expressing the evolution of the density operator by a differential equation, let us analyze if the evolution of an open quantum system can be described as a Markovian process[6], i.e. *local in time*. The reasons of this lie in the fact that if we want that a (first order) differential equation in $t$ governs the evolution of $\rho(t)$, $\rho(t+dt)$ must be completely determined by $\rho(t)$.

So, a problem emerges: an open system is *dissipative*, in the sense that information can flow from the system into the environment but also can flow back from the environment into the system, causing non-Markovian fluctuations. This fact seems to outdistance the possibility of applying the Markovian model. A possible solution is neglecting the typical correlation time of the fluctuations respect to the time scale of the evolution that we want to study.

[4] A detailed proof of the properties can be found in [36].

[5] In fact, the map satisfies a stronger property, i.e. it is completely positive; this means that if $\varepsilon$ has an operator-sum representation with Kraus operators $\{M_a\}$, then $\varepsilon \otimes \mathbb{1}$ has an operator-sum representation with Kraus operators $\{M_a \otimes \mathbb{1}\}$.

[6] Let us recall what a Markovian process is: a stochastic process is a Markovian process if the probability that the random variable $X$ takes the value $x_n$ at an arbitrary time $t_n$, is conditioned only by the value $x_{n-1}$ that it took at time $t_{n-1}$ and does not depend on the values at earlier times.

### 1.2.3 The Lindblad Master Equation

Once we take for granted that the dynamics is Markovian, we can write the evolution for the infinitesimal time interval $dt$:

$$\rho(t+dt) = \varepsilon_{dt}[\rho(t)]. \tag{1.40}$$

Expanding $\varepsilon_{dt}$ to first order, we get:

$$\varepsilon_{dt} = \mathbb{1} + dt\mathcal{L}, \tag{1.41}$$

and we find

$$\dot{\rho} = \mathcal{L}[\rho], \tag{1.42}$$

where the linear map generating time evolution $\mathcal{L}$ is called *Liouvillian* or *Lindbladian*. The quantum channel 1.41 has the operator-sum representation

$$\varepsilon_{dt}[\rho(t)] = \sum_a M_a \rho(t) M_a^\dagger = \rho(t) + \mathcal{O}(dt). \tag{1.43}$$

So we may assume that $M_0 = \mathbb{1} + \mathcal{O}(dt)$ and the $M_a$ is of order $\sqrt{dt}$ for $a > 0$. In particular, we can write:

$$M_0 = \mathbb{1} + (-iH + K)dt \tag{1.44}$$

$$M_a = \sqrt{dt}L_a, \qquad a = 1, \ldots, N^2 - 1 \tag{1.45}$$

where $H$, $K$ are both hermitian, $L_a$, H, K are zeroth order in $dt$ and $N$ is the dimension of the Hilbert space. Now, we can determine $K$ using the completeness relation 1.38:

$$\begin{aligned} \mathbb{1} &= \sum_{a=0}^{N^2-1} M_a^\dagger M_a \\ &= M_0^\dagger M_0 + \sum_{a=1}^{N^2-1} L_a^\dagger L_a dt \\ &= \mathbb{1} + 2Kdt + \sum_{a=1}^{N^2-1} L_a^\dagger L_a dt + \mathcal{O}(dt^2), \end{aligned} \tag{1.46}$$

so, keeping terms up to linear order in $dt$ we have:

$$K = \frac{1}{2}\sum_{a=1}^{N^2-1} L_a^\dagger L_a.$$

Substituting in equation 1.43, we obtain the *Lindblad master equation*[7]:

$$\dot{\rho} = \mathcal{L}[\rho] \equiv -i[H,\rho] - \sum_{a=1}^{N^2-1} \gamma_a \Big( \frac{1}{2} L_a^\dagger L_a \rho + \frac{1}{2} \rho L_a^\dagger L_a - L_a \rho L_a^\dagger \Big). \tag{1.47}$$

This is the equation that governs the evolution of a quantum system, with the assumption that the evolution is a TPCP map. The quantities $\gamma_a$ are non-negative

[7] The derivation of the master equation developed is not formally rigorous; for a more mathematically accurate derivation we refer to [6].

numbers that have the dimension of an inverse time and have the physical meaning of dissipation rate.

It is clear that the first term of equation 3.1 represents the unitary part of the dynamics generated by the Hamiltonian; the second part, instead, describes the possible evolution that the system may endure due to the interaction with the environment. Indeed, the $L_a$ are called *quantum jump operators* or *Lindblad operators*.

## 1.3 Quantifying Correlations in Quantum Systems

In this section, we introduce some tools useful to better understand quantum systems.

### 1.3.1 Bipartite Pure States

#### Schmidt Decomposition and Entanglement

A very useful tool is the *Schmidt decomposition*, that we present here following the line of reasoning of [34].

**Theorem 1.3.1.** *Let us suppose that $|\Psi\rangle$ is a pure state of a composite system $AB$, that lives in the Hilbert space given by the tensor product $\mathcal{H}_A \otimes \mathcal{H}_B$. Then there exist orthonormal bases, the Schmidt bases, $\{\chi_i^{(A)}\}$ and $\{\chi_j^{(B)}\}$, in $\mathcal{H}_A$ and $\mathcal{H}_B$, respectevely, such that*

$$|\Psi\rangle = \sum_i \alpha_i \, |\chi_i^{(A)}\rangle \otimes |\chi_i^{(B)}\rangle \, . \tag{1.48}$$

*The $\alpha_i$ are complex numbers called Schmidt coefficients and the number of non-zero $\alpha_i$ is called Schmidt number.*

*Proof.* Let $|\chi_j\rangle$ and $|\chi_k\rangle$ be orthonormal bases for systems $A$ and $B$, respectevely. So, $|\Psi\rangle$ can be written as $|\Psi\rangle = \sum_{jk} a_{jk} \, |\chi_j\rangle \, |\chi_k\rangle$. Using the singular value decomposition, we can write the matrix $a$ constituted by the elements $a_{jk}$, in this way: $a = udv$, where $d$ is a diagonal matrix with non-negative elements, $u$ and $v$ are unitary matrices. So we have $|\Psi\rangle = \sum_{ijk} u_{ji} d_{ii} v_{ik} \, |\chi_j\rangle \, |\chi_k\rangle$. Defining $|\chi_i^{(A)}\rangle \equiv \sum_j u_{ji} \, |\chi_j\rangle$, $|\chi_i^{(B)}\rangle \equiv \sum_k v_{ik} \, |\chi_k\rangle$ and $\alpha_i \equiv d_{ii}$, we get $|\Psi\rangle = \sum_i \alpha_i \, |\chi_i^{(A)}\rangle \otimes |\chi_i^{(B)}\rangle$. □

A state $|\Psi\rangle \in \mathcal{H}_A \otimes \mathcal{H}_B$ is said to be *entagled* if it **cannot** be written as a tensor product $|\chi^{(A)}\rangle \otimes |\chi^{(B)}\rangle$ of states of the sub-systems, i.e. if the Schmidt number is greater than 1. Moreover, if the absolute values of all non-vanishing Schmidt coefficients are equal to each other the state $|\Psi\rangle$ is said to be *maximally entangled*. Conversely, if a state $|\Psi\rangle$ **can** be written as a tensor product is named *product state* and this is true if and only if the Schmidt number is equal to 1. We can say that the Schmidt number is a measure of the entanglement between the system $A$ and the system $B$.

#### Von Neumann Entropy

A crucial tool useful to measure the entanglement of a bipartite pure state is the quantum entropy, defined by von Neumann in this way:

$$S(\rho) \equiv -\operatorname{Tr}(\rho \log_2 \rho), \tag{1.49}$$

where $\rho$ is the state of the system. If $\lambda_i$ are the eigenvalues of $\rho$, we can write:

$$S(\rho) = -\sum_i \lambda_i \log_2 \lambda_i.$$

Let us highlight some important properties of the von Neumann entropy [34, 6]:

- $S(\rho) \geq 0$, where the equality sign holds if and only if $\rho$ is a pure state;
- in a D-dimensional Hilbert space, the entropy is $S(\rho) \leq log_2 D$, where the equality sign holds if and only if the system in the completely mixed state $\rho = \mathbb{1}/D$;
- if a composite system $AB$ is in a pure state, $S(A) = S(B)$;
- it is a concave functional $\rho \mapsto S(\rho)$ on the space of density matrices. This means that for any collection of $\rho_i$ and numbers $\lambda_i$ satisfying $\sum_i \lambda_i = 1$, one has $S(\sum_i \lambda_i \rho_i) \geq \sum_i \lambda_i S(\rho_i)$, where the equal sign holds if and only if all $\rho_i$ are equal to each other. This property means that the uncertainty of the state $\rho = \sum_i \lambda_i \rho_i$ is greater or equal to the average uncertainty of the states $\rho_i$ that constitute the total mixture;
- if $\rho$ associated to Hilbert space $\mathcal{H} = H_A \otimes H_B$ is the state of a system and $\rho^{(A)} = \mathrm{Tr}_B \rho$ and $\rho^{(B)} = \mathrm{Tr}_A \rho$ are the states of its sub-systems, the von Neumann entropy obeys the so-called subadditivity condition, i.e.

  $$S(\rho) \leq S(\rho^{(A)}) + S(\rho^{(B)}),$$

  where the equality sign holds if and only if $\rho$ describes an uncorrelated state. This means that the uncertainty about the product state is greater than that of the total system; this is because the operation of trace over the sub-systems causes a loss of information on correlations between the sub-systems, therefore the increase of entropy.

A comprehensive review that explains several kind of measures of entanglement in many-body systems is the ref. [1].

# Chapter 2

# Quantum Simulators of Open Many-Body Quantum Systems

> Can a quantum system be probabilistically simulated by a classical universal computer? [...] The answer is certainly, no!
>
> *Richard P. Feynman*

Open many-body quantum systems represent a challenging area of study, due to the exponential growth of the number of freedom degrees with respect to the number of the constituent particles. The scientific community has built many strategies to overcome this obstacle, by developing and refining several analytical and numerical methods. In addition to these, another approach was proposed, based on the use of quantum simulators.

In the present chapter it is reported a review of some of the most relevant idea in the field of quantum simulators; in particular, the last section focuses on the simulation of spin systems, of remarkable interest in view of the model studied in this work.

## 2.1 Quantum Many-Body Systems

Quantum many-body systems are systems made up by a certain number of interacting particles. Typical quantum many-body systems are represented by Hubbard-like models or spin chains. A prototype of these systems is described by the non-dissipative Bose-Hubbard model [16]: an interacting boson gas in a lattice potential. The hamiltonian reads:

$$H = -J \sum_{\langle i,j \rangle} \hat{a}_i^\dagger \hat{a}_j + \sum_i \epsilon_i \hat{n}_i + \frac{1}{2} U \sum_i \hat{n}_i (\hat{n}_i - 1), \tag{2.1}$$

where $\hat{a}_i$ and $\hat{a}_i^\dagger$ are the bosonic creation and annihilation operators respectively, on the i-th site; $\hat{n}_i$ is the number operator, which counts the number of bosons in the i-th site; $\epsilon_i$ is the energy due to the external harmonic confinement to which the bosons are undergone. The $J$ term is the one responsible for the hopping between adjacent sites due to the tunnel coupling; it is the matrix element:

$$J = -\int d^3x \quad w(\vec{x} - \vec{x}_i)(-\frac{\nabla^2}{2m} + V(\vec{x}))w(\vec{x} - \vec{x}_j),$$

where $w(\vec{x} - \vec{x}_i)$ is a single particle Wannier function localized to the i-th site, $V(\vec{x}))$ is the lattice potential and $m$ is the mass of a single boson. $U$ is instead the matrix element for the interaction between bosons in the same site; it is:

$$U = \frac{4\pi a}{m} \int d^3x \quad |w(\vec{x})|^4,$$

$a$ being the scattering length.

If the tunnel coupling term $J$ dominates the hamiltonian, the ground-state energy is minimized if the single-particle wavefunctions of the $N$ bosons is spread out over the entire $M$ sites of the lattice; so the many-body ground state reads:

$$|\Psi_{SF}\rangle \propto \Big(\sum_{i=1}^{M} \hat{a}_i^\dagger\Big)^N |0\rangle\,,$$

i.e. all bosons occupy the same extended Bloch state. As pointed out by [16], an important feature of this state is that the probability distribution of the occupation $n_i$ of bosons on a single site is poissonian, so that its variance is given by $\langle n_i \rangle$; this means that it is well described by a macroscopic wavefunction with long-range phase coherence throughout the lattice.

If the on-site intraction term $U$ dominates the hamiltonian, the ground state of the system will instead consist of localized wavefunctions with a fixed number of bosons per site that minimized the energy; the many-body ground state will be a product of local Fock states for each site:

$$|\Psi_{MI}\rangle \propto \prod_{i=1}^{M} \Big(\hat{a}_i^\dagger\Big)^N |0\rangle\,.$$

The two kind of ground state have been labeled with the subscripts "SF" and "MI", specifying the two phases to which the system may do the transition: superfluid and Mott insulator phases.

## 2.2 Quantum Simulators: Controllable Many-Body Systems

In order to overcome the mentioned problem, over the years several analytical and numerical methods have been developed. In addition to these more "traditional" approaches, during the last years it arose the idea of studying a quantum system by using a properly designed quantum device. The essential aim of this new strategy lies in the employment of controlled quantum devices called *quantum simulators*; they are systems able to experimentally emulate the Hamiltonian model bearing the non-trivial properties of the system under study. The usefulness of this approach is twofold [49]: not only it allows to explore properties of the model in regions that are elusive to the analytical and numerical studies, but also it consents to test to which limits the Hamiltonian model is appropriate to describe the system or whether additional ingredients are required.

Since the Josephson junction arrays [13], that were probably the first quantum simulators in Physics History, much progress have been made especially with the advent of cold atoms in optical lattices.

### 2.2.1 Cold Atoms in Optical Lattices

[H]

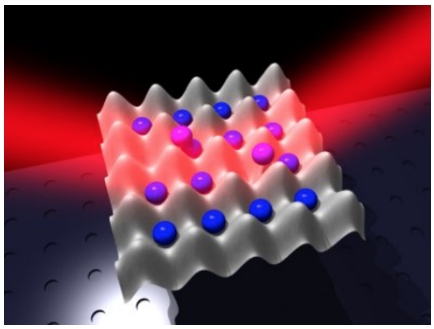

FIGURE 2.1: Optical lattices are crystals made of light: lasers beams interfere to form a periodic potential in which ultracold atoms are trapped. Figure taken from LENS laboratory, Florence [27].

The employment of cold atoms in optical lattices has proved to be a successful way to create simulators of a large variety of strongly interacting systems [28].

In short, optical lattices are created by making laser beams counter-propagating interfere with each other [17]. The result is a standing wave with a periodic pattern (see sketch in fig. 2.1). Then, ultracold atoms can be trapped in the potential wells, creating first a Bose-Einstein condensate or a cold gas of fermionic atoms and then slowly ramping up the laser beams to create the periodic lattice potential.

Ultracold atoms in optical lattices represent nearly perfect realization of fermionic and bosonic Hubbard models[1] [28] and they are usually employed to simulate non-dissipative systems. However, new efforts have been made in order to introduce dissipation in these devices. In fig. 2.2, a sketch of the implementation of the effective dissipative process in an optical *superlattice* is shown. The so-called superlattice is made up coupling driven-dissipative ultracold atoms in an optical lattice with a coherently driven reservoir.

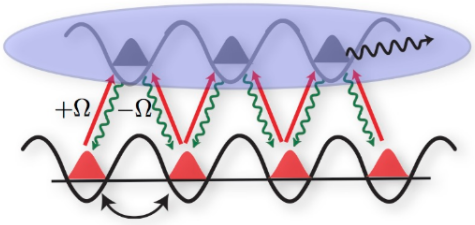


FIGURE 2.2: Schematic realization of the effective dissipative process with ultracold atoms in an optical superlattice. Figure taken from [22].

An interesting study over the possibility of using cold atoms to simulate dissipative many-body systems, has been done by [12]. In this work, they discuss the example of a driven dissipative Bose-Einstein condensate of bosons, where atoms in optical lattice are coupled to a bath of Bogoliubov excitations; the atomic current

[1]The (fermionic) Hubbard model in one dimension is characterized by the following Hamiltonian:

$$\mathcal{H} = -t \sum_{\langle ij \rangle} a^{\dagger}_{i\sigma} a_{j\sigma} + U \sum_{i} n_{i\uparrow} n_{i\downarrow},$$

where the first term represents the hopping between adjacent sites and the second represents the on-site interaction between particles. The $n_{i\sigma}$ are the occupation numbers, that count the number of electron with spin $\sigma$ in site $i$. In the text, the plural *Hubbard models* refers to the several variations of this model.

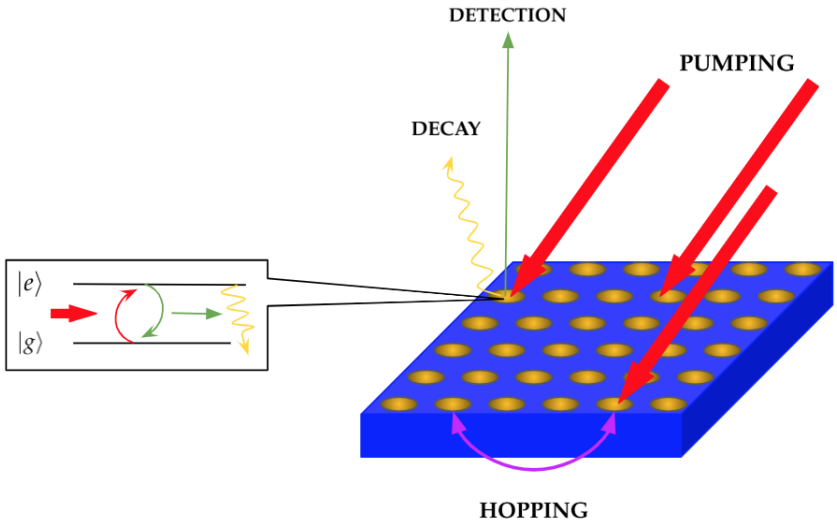


FIGURE 2.3: Sketch of array of QED cavities. In the inset there is a draft of the interaction between the two-level system and the photon resonating in the cavity and then decaying. Photons in the cavities have finite life-time, so there is a coherent external drive.

represents local dissipation. It was assumed that the atoms can be described by a Hubbard model, having the following Hamiltonian:

$$\mathcal{H} = \mathcal{H}_0 + V \equiv -J \sum_{\langle i,j \rangle} a_i^\dagger a_j + \frac{1}{2} U \sum_i a_i^{\dagger 2} a_j^2, \tag{2.2}$$

where $\mathcal{H}_0$ represents the kinetic energy of bosons hopping between adjacent lattice sites with amplitude J, V is the onsite interaction with strength U and $a_i$ ($a_i^\dagger$) are bosonic destruction (creation) operators for atoms at i-th site. At this point, an appropriate choice of jump operators allows to couple the system to a bath so that it is driven to a pure many-body state by quasi-local dissipation. Applying standard linearization schemes in the weakly interacting situations led to obtain the solution of the master equation 3.1. The steady-state solution seems to have properties similar to those of bosons in thermal contact to a heat bath.

Another strategy involves trapping Rydberg atoms in optical lattices. Rydberg atoms are alkali-like atoms with a single electron promoted into a highly excited orbital [9]. The presence of this atoms enhances photon-photon interaction; the presence of a single photon in the system is able to drive away from resonance condition all atoms contained in a surrounding volume. If the optical density is sufficiently high, a second photon travelling across this volume can be absorbed or suffer a phase shift; this can be use to obtain an effective blockade effect.

### 2.2.2 QED-Cavity Arrays

In the last few decades the field of quantum simulators has been enriched by a new idea, based on arrays of QED cavities [49] (sketched in fig. 2.3), in which light resonates and interacts with matter contained therein. A compelling aspect of this kind of devices is the competition between two phenomena: while on the one hand light-matter interaction inside the cavity leads to photon blockade, on the other photon hopping between neighbouring cavities favors delocalization.

QED cavities are mathematically described by the Jaynes-Cummings model [48], in which one mode of the cavity interacts with a two-level system. By ignoring light-matter interaction, a single cavity confines several modes of electromagnetic field and each of them is quantized as a harmonic oscillator. If one considers a cavity with a single mode with frequency $\omega$, the Hamiltonian describing such a system can be written as

$$\mathcal{H} = \omega a_l^\dagger a_l, \tag{2.3}$$

where $a_l(a_l^\dagger)$ annihilates (creates) a quantum of light in the mode of the l-th cavity. An array of cavities sufficiently close to allow for photon hopping, can be described by eq. 2.3 to which the following term should be added:

$$\mathcal{H}_{hop} = -J(a_l^\dagger a_{l+1} + h.c.),$$

where J is associated with the tunneling rate. Now, if the light-matter interaction is introduced, the Hamiltonian can be written in this way:

$$\mathcal{H} = \sum_l \mathcal{H}_l^{(0)} - J \sum_{\langle l,l' \rangle} (a_l^\dagger a_{l'} + h.c.), \tag{2.4}$$

where the term $\mathcal{H}_l^{(0)}$ describes the light-matter interaction. In particular, we want to study QED cavities so the Hamiltonian term $\mathcal{H}_l^{(0)}$ is the Jaynes-Cummings model:

$$\mathcal{H}_{l,JC}^{(0)} = \varepsilon \sigma_l^z + \omega a_l^\dagger a_l + g(\sigma_l^+ a_l + \sigma_l^- a_l^\dagger), \tag{2.5}$$

where $\sigma_l^\pm$ are the raising/lowering operators for the two-level system and $\varepsilon$ states the transition energy between the two levels. The spectrum of the Hamiltonian 2.5 is anharmonic, meaning the presence of the two-level system induces a repulsion between the photons in the cavity, so that in the cavity only a photon can be present at the same time. Qualitatively, this can be explained by the fact that a single photon in the cavity modifies the effective resonance frequency, so that the injection of another photon is inhibited. This nonlinear process is known as *photon blockade* and has been named in analogy of the Coulomb blockade effect of electron transport through mesoscopic devices.

An array of cavities in the impenetrable photon regime has been theoretically studied [9]. As sketched in fig. 2.4, a continuous pumping is considered. The transmission and/or absorption spectrum of the system shows the Tonks-Girardeau nature of the steady-state of photon gas, i.e. the fermionization of photons.

### 2.2.3 Superconducting Circuits

As for QED-cavities, also for superconducting circuits, or QED-circuits, light-matter interaction is central. In this simulators [20], the quantum "particles" are excitations, not physical particles subjected to conservation laws, so they naturally access non-equilibrium physics. Photonic mode can be realized with on-chip microwave resonators, typically Fabry-Perot kind of cavities. A qubit coupled to such a resonator can be described by the Jaynes-Cummings model:

$$\mathcal{H}_{JC} = \omega_r a^\dagger a + \varepsilon \sigma^+ \sigma^- + g(a\sigma^+ + a^\dagger \sigma^-), \tag{2.6}$$

where $\omega_r$ and $\varepsilon$ are the the photon and qubit excitation frequencies, and $a^\dagger$, a, $\sigma^+$ and $\sigma^-$ denote the corresponding raising and lowering operators. An example of these

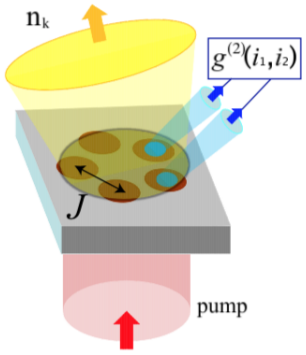


FIGURE 2.4: Sketch of an array of five cavities arranged in a ring geometry with periodic boundary conditions; the system is driven by a laser. Figure taken from [9].

devices can be seen in fig. 2.5.

### 2.2.4 Arrays of Optomechanical Systems

A recent proposal by [31] considers making arrays of optomechanical systems. The essential idea is that at each site of such an array, a localized mechanical mode interacts with an optical mode of a cavity driven by laser beams; the interaction occurs via radiation pressure. This way, both photons and phonons can hop between neighbouring sites. Because of the experimental complexity of this kind of device, only a single cavity has been cooled to the ground state [26], so far.

The work of [31] focuses on the transition of the collective mechanical motion from an incoherent state (due to quantum noise) to an ordered state with phase-coherent mechanical oscillations; for this dynamics, the dissipative effects induced by the optical modes play a crucial role. Indeed, they allow the mechanical modes to have self-induced oscillations, once the optomechanical amplification rate exceeds the intrinsic mechanical damping; on the other hand, the quantum noise prevents the mechanical modes to synchronizing.

## 2.3 Quantum Simulation of Spin Systems

Interacting two level systems, either spins or qubits, are of central importance in Quantum Information and Condensed Matter Physics.

Since the discover of the *photon blockade* [21] arose the fact that the cavity mode is well described by a spin-1/2 Hamiltonian. Few years later, the Jaynes-Cummings model in the Mott regime was shown to simulate a XY spin model [2]. In particular, the studied system consisted of coupled electromagnetic cavities doped with single two-level system; it is shown the possibility of observing an insulator phase of total (atomic plus photonic, i.e. *polaritonic*) excitations. From such a system, an effective XY Hamiltonian arises, with spin up (down) corresponding to the presence (absence) of a polariton.

A scheme for realizing the Ising spin-spin interaction has been proposed in [30], where a system consisting in trapped two-level atoms in a one dimensional coupled microcavities.

A more complicated system has been investigated in [18], which uses three-level atoms in micro-cavities coupled to each other via the exchange of virtual photons; it

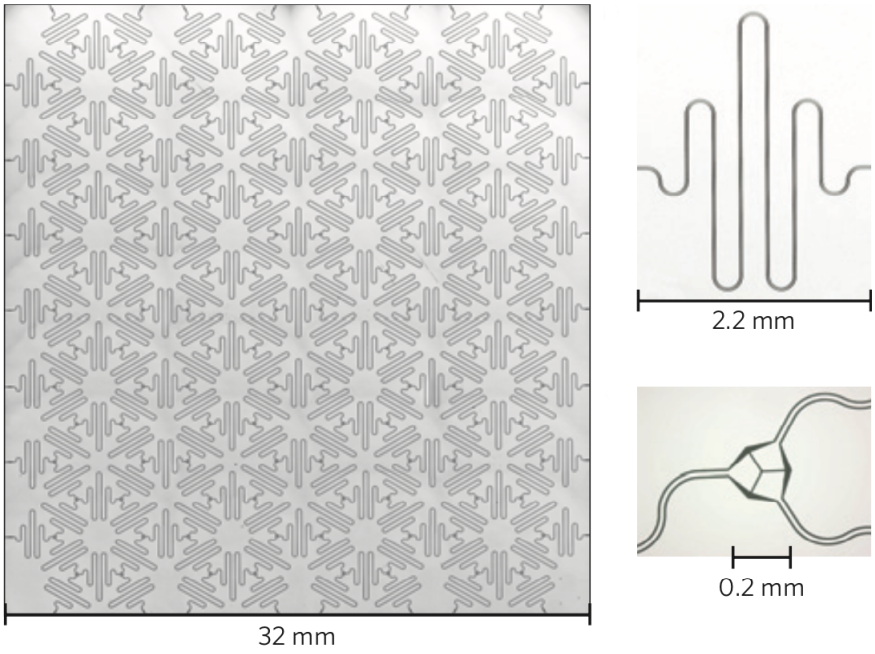


FIGURE 2.5: Example of an array of resonators forming a honeycomb pattern. On the left, more than two hundred microwave cavities are coupled in a Kagome lattice, a natural two-dimensional lattice. Each cavity is coupled to two neighbours, through a capacitor that enables photon hopping. On the bottom-right, it can be seen the simmetric three-way capacitor that ensures uniform hopping rates throughout the array. Figure taken from [20].

is shown that it can model an anisotropic Heisenberg spin-1/2 chain in an external magnetic field. The two spin polarizations $|\uparrow\rangle$ and $|\downarrow\rangle$ are represented by two long-lived atomic levels of a $\Lambda$ level-structure; let us see why. The quantized mode of the cavity together with external lasers can induce Raman transition between these two lowest-lying states. With appropriately chosen detunings, the dominant Raman transition between the two lowest-lying states involves one laser and one cavity photon. This implies that the emission and absorption of virtual photons in the cavity is confined to only two states per atom, the long-lived ones, so that can be described by a spin-1/2 Hamiltonian. The coupling of virtual photons between neighbouring cavities simulates $\sigma^x\sigma^x$ and $\sigma^y\sigma^y$ interactions; the effective spin can be coupled to an effective magnetic field $\sigma^z$; using the same atomic level configuration but a different set-up of the external sources an effective $\sigma^z\sigma^z$ interaction is obtained.

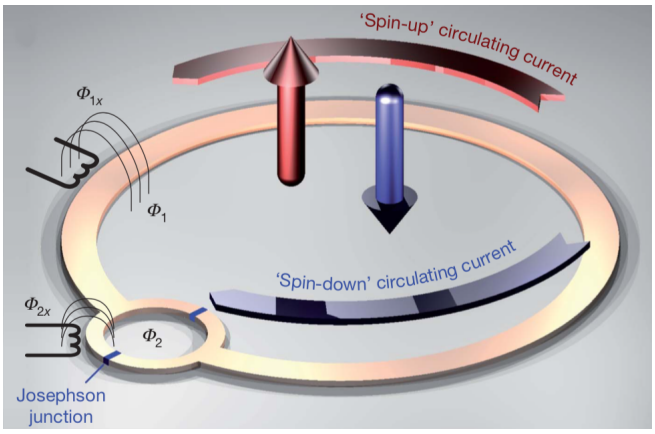


FIGURE 2.6: Simplified schematic of a superconducting flux qubit acting as a quantum mechanical spin [24].

It has been possible using superconducting circuits to simulate small spin chains, by directly coupling a number of superconducting qubits [24]. Fig.2.6 shows two superconducting loops in the qubit, each subject to an external flux bias $\Phi_{1x}$ and $\Phi_{2x}$. The dynamics of the device can be modelled as a quantum mechanical double-well potential. The two lowest energy states of the system correspond to clockwise or anticlockwise circulating current in loop 1. Considering only these two states (in the limit of low temperature it is a valid approximation), the qubit dynamics is that of an Ising spin. Qubits are then coupled together using programmable coupling elements; this allows to tune the spin coupling in a continous way between ferromagnetic and antiferromagnetic. The behaviour of this system is well described by an Ising model Hamiltonian:

$$\mathcal{H} = \sum_{i=1}^{N} h_i \sigma_i^z + \sum_{i,j=1}^{N} J_{ij} \sigma_i^z \sigma_j^z.$$

In this way, it has been possible to simulate a one-dimensional 8-sites spin chain, with the ends polarized in opposite directions.

# Chapter 3

# Numerical Methods for Open Quantum Systems

Hilbert space is a big place.

*Carlton Caves*

As we have seen in the previous chapter, the study of an open quantum system requires the knowledge of its density matrix, solution of the Lindblad master equation [36]:

$$\dot{\rho} = \mathcal{L}[\rho],$$

where

$$\mathcal{L}[\rho] \equiv -i[H,\rho] - \sum_{a=1}^{N^2-1} \gamma_a \Big( \frac{1}{2} L_a^\dagger L_a \rho + \frac{1}{2} \rho L_a^\dagger L_a - L_a \rho L_a^\dagger \Big), \tag{3.1}$$

$N$ being the dimension of Hilbert space.

In such a system the number of variables scales as the square of the dimension of the Hilbert space; for example, in a spin-$\frac{1}{2}$ system made up by $n$ elements, the size of the Hilbert space $\mathcal{H}$ is $2^n$ while the *liouvillian dimension* equals to $2^{2n} \times 2^{2n}$. Clearly, a direct integration of the equation 3.1 can be made only for systems with a very limited number of elements. One only needs to note the fact that for a brute-force integration of the equation 3.1 for a system consisting of 8 sites, about 34 GB of memory would be necessary[1].

Nevertheless, some techniques for exact diagonalization of Liouvillian superoperator 3.1 has been developed. To name but one, that devised by Prosen in [38] for studying a system characterized by a quadratic Hamiltonian and linear Lindblad operators, prescribes to diagonalize the Liouville super-operator in terms of $2n$ normal master modes, i.e. anticommuting super-operators which act on the Fock space of density operators. This can be understood as a complex version of Bogoliubov transformation.

However, as seen previously, a direct integration of master equation for an open many-body system becomes unfeasible even for relatively small sizes, so conceiving numerical strategies seems to be necessary.

One of them is based on the *mean field* approach; the essential idea is considering the mean value of the Hamiltonian and, as suggested by Gutzwiller, factorizing the density matrix, defining a mean field density matrix $\rho_{MF} = \prod_j \rho_j$, where $\rho_j$ is the single site density matrix. In this way, all correlations and interactions between sites are neglected, so we can say it is a crude approximation for an interacting many-body system. In order to (partially) overcome this problem, the *cluster mean field*

[1] This calculation considers the fact that the liouvillian contains, in general, complex numbers, each of them valued with a single precision (32 bit).

method was developed: in this method a set of contiguous sites are isolated from the rest of the system. As explained in [23], this method suggests to write the Hamiltonian as $H_{CMF} = H_{\mathcal{C}} + H_{\mathcal{B}(\mathcal{C})}$, where the first term describes the exact interactions inside the cluster while the second term represents the mean-field interactions between the cluster and the sites on its boundary $\mathcal{B}(\mathcal{C})$. The global density matrix will be $\rho_{CMF} = \bigotimes \rho_{\mathcal{C}}$, where the $\rho_{\mathcal{C}}$ is the density matrix of the $\mathcal{C}$-th cluster. One should note that, when the cluster is made up by a single site, the method becomes the above-mentioned standard one.

Others important numerical methods are the ones essentially based on the *linked cluster expansions* [57], in which the quantities of interest are expressed as sums of contributions from a sequence of clusters of sites; in particular, only connected clusters contribute. In [29] an application of this idea to the Liouvillian is done.

In this section, we will examine some of the numerical techniques used for studying open quantum systems with very different approaches.

Two of the three numerical methods analyzed in this chapter are essentially based on the Wilson's *renormalization group* approach [55] combined with the fundamental contribution of the White's *density matrix renormalization group* (DMRG) method [53] and are the *corner-space renormalization* and the *matrix product density operators* methods. They both use the idea of a system decomposition into blocks; even if the basic idea is the same, the developed approaches are actually different.

The first numerical method analyzed in the section 3.1 is the *quantum trajectories* method, based on the evolution of a Monte Carlo wave function.

## 3.1 The Quantum Trajectories (QT) Method

The *quantum trajectories method* is an estabilished numerical method, in which pure states are the subjects of the study, instead of density matrices. This means that, if the Hilbert space has dimension $N$, the number of involved parameters ($\sim N$) is much smaller than the one required in calculations with density matrices ($\sim N^2$). This method was originally proposed in 1992 by Dalibard, Castin and Mølmer in [11], then generalized in [33], as a stochastic unraveling of the master equation, namely a stochastic evolution for the wave function of a system coupled to a reservoir. It has been proved [11, 33] the equivalence of this *Monte Carlo wave-function* approach with the master equation treatment.

The idea of this method can be summarised in the following way.

First of all, given the 3.1, let us note that the first three terms of this equation can be regarded as the evolution performed by an effective non-Hermitian Hamiltonian, that is [8]:

$$H_{\text{eff}} = H_s + \mathrm{i}K,$$

with

$$K = -\frac{1}{2}\sum_{\mu} L_{\mu}^{\dagger} L_{\mu}.$$

Indeed, we see that:

$$-\mathrm{i}[H_{\text{eff}}, \rho] = -\mathrm{i}[H_s, \rho] - \frac{1}{2}\sum_{\mu}\{L_{\mu}^{\dagger} L_{\mu}, \rho\}.$$

The summation term in the 3.1, is the one responsible for the so-called *quantum jumps*; for this reason, the representation under which we have written the 3.1 is called *quantum jump picture* [8].

At an initial time $t_0$, the density matrix of the system is in a pure state

$$\rho(t_0) = |\phi(t_0)\rangle \langle\phi(t_0)| ;$$

after a time $dt$, it evolves to the following statistical mixture:

$$\rho(t_0 + dt) = \Big(1 - \sum_\mu dp_\mu\Big) |\phi_0\rangle \langle\phi_0| + \sum_\mu dp_\mu |\phi_\mu\rangle \langle\phi_\mu| , \tag{3.2}$$

where

$$dp_\mu = \langle\phi(t_0)| L_\mu^\dagger L_\mu |\phi(t_0)\rangle \, dt \tag{3.3}$$

is the probability that a jump occurs; in this case, the system evolves in the state

$$|\phi_\mu\rangle = \frac{L_\mu}{L_\mu |\phi(t_0)\rangle} |\phi(t_0)\rangle . \tag{3.4}$$

Otherwise, if no jump happens, the system evolves according to the effective Hamiltonian $H_{eff}$ in the following way:

$$|\phi_0\rangle = \frac{(1 - \mathrm{i} H_{eff} dt)}{\sqrt{1 - \sum_\mu dp_\mu}} |\phi(t_0)\rangle . \tag{3.5}$$

In order to decide if the jump occurs or not, a Monte Carlo method will be integrated in this picture. Namely, an uniform distribution in the unit interval $[0, 1]$ is taken under consideration; for every experiment, a pseudo-random number $\epsilon$ is chosen from this uniform distribution, i.e. a coin is tossed: depending on the result of the throw, the possible situations are the following:

- if $\epsilon < \sum_\mu dp_\mu$, the system jumps to one of the states $|\phi_\mu\rangle$, defined in 3.4. In particular:
  - if $0 \leq \epsilon \leq dp_1$, the system jumps to $|\phi_1\rangle$;
  - if $dp_1 < \epsilon \leq dp_2$, the system jumps to $|\phi_2\rangle$;
  - and so on;
- if $\epsilon > \sum_\mu dp_\mu$, the system evolves to the state $|\phi_0\rangle$.

This process has to be repeated as many times as $n = \frac{T}{dt}$, where $T$ is the whole elapsed time during the evolution. Let us note that $dt$ must be taken much smaller than the scales relevant for the evolution of the system.

Every *experiment*, i.e. every throw of the coin, gives a different *quantum trajectory*, which can be used to calculate the mean value of an observable $A$ at a certain time $t$, in this way:

$$\langle A(t)\rangle = \langle\phi_i(t)| A |\phi_i(t)\rangle . \tag{3.6}$$

Since this results from a Monte Carlo process, we can consider the mean value over $N$ *experiments*:

$$\langle A(t)\rangle = \lim_{N\to\infty} \frac{1}{N} \sum_{i=1}^{N} \langle\phi_i(t)| A |\phi_i(t)\rangle . \tag{3.7}$$

So, to sum up we can say a few things about QT algorithm; it allows to do the so-called *stochastic unraveling* of the master equation, using pure states instead of density matrices: as we have seen, this simplifies the computational complexity of

the problem. However, this method has an important limit: it does not prevent the exponential growth respect to the size of the system. Trying to work this out will be a task of the methods that will be analyzed in the next two sections.

## 3.2 The Corner-Space Renormalization (CSR) Method

The numerical methods based on renormalization group à la Wilson present a computational problem due to the increase of the dimensions of the Hilbert space, while the blocks are merged; the fundamental aim of the corner-space renormalization (CSR) method [14] is to deal with this problem and try to overcome the limitation mentioned above.

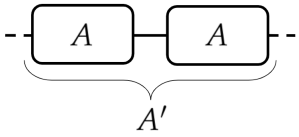


FIGURE 3.1: Blocking scheme of Wilson's NRG method.

First of all, it is important to mention Wilson's numerical renormalization group (NRG) procedure, in which the CSR method is rooted.

Let us consider a 1D-system made up by $N$ spins. The NRG method suggests to take two spins and consider a subspace of the corresponding Hilbert space $\mathcal{H}_2 \subset \mathcal{H}_1 \otimes \mathcal{H}_1$ of dimension $d_2 \leq d_1^2$; then, one adds a spin and consider the subset of the Hilbert space of three spins $\mathcal{H}_3 \subset \mathcal{H}_2 \otimes \mathcal{H}_1$ of dimension $d_3 \leq d_2 d_1$, and so on until one arrives to consider the subset of Hilbert space $\mathcal{H}_N \subset \mathcal{H}_{N-1} \otimes \mathcal{H}_1$ with dimension $d_N \leq d_{N-1} d_1$. So, one can approximate the Hamiltonian with $P_N H P_N$, where the $P_N$ is the projector onto $\mathcal{H}_N$. If one chooses $d_N$ sufficiently small, one can diagonalize the Hamiltonian and find eigenvalues and eigenvectors. A good thing to do is fixing for all the dimensions $d_n$ the so-called *bond dimension* such that

$$d_n \leq D \quad \forall \quad n.$$

Considering a one-dimensional spin chain, the NRG method requires to break the chain into a set of identical blocks A (see fig. 3.1). So, one diagonalizes the Hamiltonian matrix $H_{AA}$ for two neighboring blocks $A$ and uses its lowest $m$ eigenstates (ordered by energy) to form a pseudo-unitary matrix $O$, employed to change the basis and make up the Hamiltonian $H_{A'}$ representing the block $A'$ twice as large (see fig. 3.1), in this way:

$$H_{A'} = O H_{AA} O^{\dagger},$$

where $O$ is a $m \times n$ matrix (the rows of $O$ are the $m$ lowest eigenstates of $H_{AA}$) and $H_{AA}$ has dimension $n \times n$. This procedure has to be repeated using the new larger blocks $A'$ and the new effective Hamiltonian $H_{A'}$.

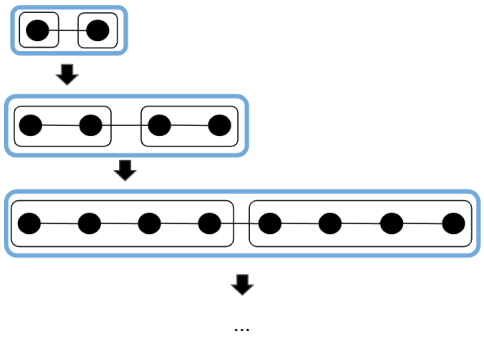

FIGURE 3.2: Merging of the blocks in NRG procedure.

It is worth noting that the NRG method overlooks the connections between the blocks (see fig. 3.2), so it is a good method only in the limit that the links between the blocks vanish. This weak point has been studied and overcome by White in [53] where he developed the DMRG method, that will be outlined in the following section.

The CSR method can be seen as a generalization of the NRG method, a development to the case of open systems. The name refers to the idea of selecting a *corner* of the Hilbert space for a lattice system, using eigenvectors of the steady-state density matrix of smaller lattices.

Let us start considering two blocks of a quantum system consisting in a certain number $N$ of sites. The CSR approach is a recursive process that begins with the calculation of the steady-state density matrix of a small block (the first *block* will be a single site, in the second iteration it will be a small lattice constituted of the two blocks emerged in the previous iteration, and so on); this calculation can be done studying the spectrum of the eigenvalue of the Liouvillian and taking the zero value, considered that

$$\frac{d\rho}{dt} = \mathcal{L}\rho \tag{3.8}$$

can be seen as an eigenvalue equation.

We now consider two spatially adjacent sites: the site A and the site B. We now call $\rho^{(A)}$ the steady-state density matrix of the first site and $\rho^{(B)}$ of the latter site. In order to spatially merge these two sites, let us write $\rho^{(A)}$ and $\rho^{(B)}$ in terms of an orthonormal basis; if there is no degeneracy among eigevalues of $\rho^{(A)}$ and $\rho^{(B)}$, we can use the orthonormal basis formed by their eigenvectors. Instead, if there is degeneration, a Gram-Schmidt orthonormalization process can be used to obtain an orthonormal basis starting from the ensemble of eigenvectors.

In this way, we will have:

$$\begin{aligned} \rho^{(A)} &= \sum_r p_r^{(A)} \left|\phi_r^{(A)}\right\rangle \left\langle\phi_r^{(A)}\right|, \\ \rho^{(B)} &= \sum_{r'} p_{r'}^{(B)} \left|\phi_{r'}^{(B)}\right\rangle \left\langle\phi_{r'}^{(B)}\right|, \end{aligned} \tag{3.9}$$

where

$$\begin{aligned} p_r^{(A)} \geq 0 \quad \forall r \quad \text{and} \quad p_{r'}^{(B)} \geq 0 \quad \forall r', \\ \sum_r p_r^{(A)} = 1 \quad \text{and} \quad \sum_{r'} p_{r'}^{(B)} = 1. \end{aligned}$$

The steady-state density matrix of the *merged block* constituted of the block A and the block B will be the following:

$$\rho^{(AUB)} = \rho^{(A)} \otimes \rho^{(B)} = \tag{3.10}$$

$$= \sum_r \sum_{r'} p_r^{(A)} p_{r'}^{(B)} \left|\phi_r^{(A)}\right\rangle \left|\phi_{r'}^{(B)}\right\rangle \otimes \left\langle\phi_{r'}^{(B)}\right| \left\langle\phi_r^{(A)}\right| \tag{3.11}$$

At this point, the CSR method suggests to delineate the *corner-space*; for this purpose, we consider the $M$ most probable product states coming from 3.10 of the form $\left|\phi_r^{(A)}\right\rangle \left|\phi_{r'}^{(B)}\right\rangle$, i.e. we rank the 3.11 according to the joint probability $p_r^{(A)} p_{r'}^{(B)}$. The $M$ states form an orthonormal basis that generates a subspace

$$\left\{ \left|\phi_{r_1}^{(A)}\right\rangle \left|\phi_{r'_1}^{(B)}\right\rangle, \left|\phi_{r_2}^{(A)}\right\rangle \left|\phi_{r'_2}^{(B)}\right\rangle, \ldots, \left|\phi_{r_M}^{(A)}\right\rangle \left|\phi_{r'_M}^{(B)}\right\rangle \right\}, \tag{3.12}$$

called *corner-space*, with

$$p_{r_1}^{(A)} p_{r'_1}^{(B)} \geq p_{r_2}^{(A)} p_{r'_2}^{(B)} \geq \cdots \geq p_{r_M}^{(A)} p_{r'_M}^{(B)}.$$

So, now it becomes necessary doing a change of basis to the new block $A \cup B$, that is:

$$H' = \widetilde{O} H_{A\cup B} \widetilde{O}^\dagger, \tag{3.13}$$

where $\widetilde{O}$ is a pseudo-unitary[2] $M \times N$ matrix, where $N$ is the dimension of $H_{A\cup B}$; $\widetilde{O}$ is formed by the $M$ eigenvectors of $\rho_{A\cup B}$ living in the corner-space. This density matrix can now be used to calculate the expectation values of any observable.

The more $M$ is large, the more the results are exact, because the basis 3.12 spans a larger part of the Hilbert space. Therefore, at this point the value of $M$ should be increased until the convergence is reached.

In the work of [14] it has been proved that convergence can be achieved with a number of states $M$ much smaller than the dimension of the Hilbert space. In the present thesis, it will be shown that this method can not be used for the analysis of systems described by a model such as that under consideration in the present work.

In short, the algorithm is structured in the following stages, as sketched in fig. 3.3:

**calculation** of the steady-state density matrix of a single block of the system;

**merger** of two predetermined blocks;

**expression** of the density matrix of the merged block in an orthonormal basis;

**selection** of the M most probable states as a basis for the so-called *corner-space*;

**increase** of the dimension M of the corner-space until the convergence of the observable is achieved.

A detailed description of the implementation of the algorithm can be seen in Appendix A.

[2]The matrix $\widetilde{O}$ is called pseudo-unitary because it is not a square matrix.

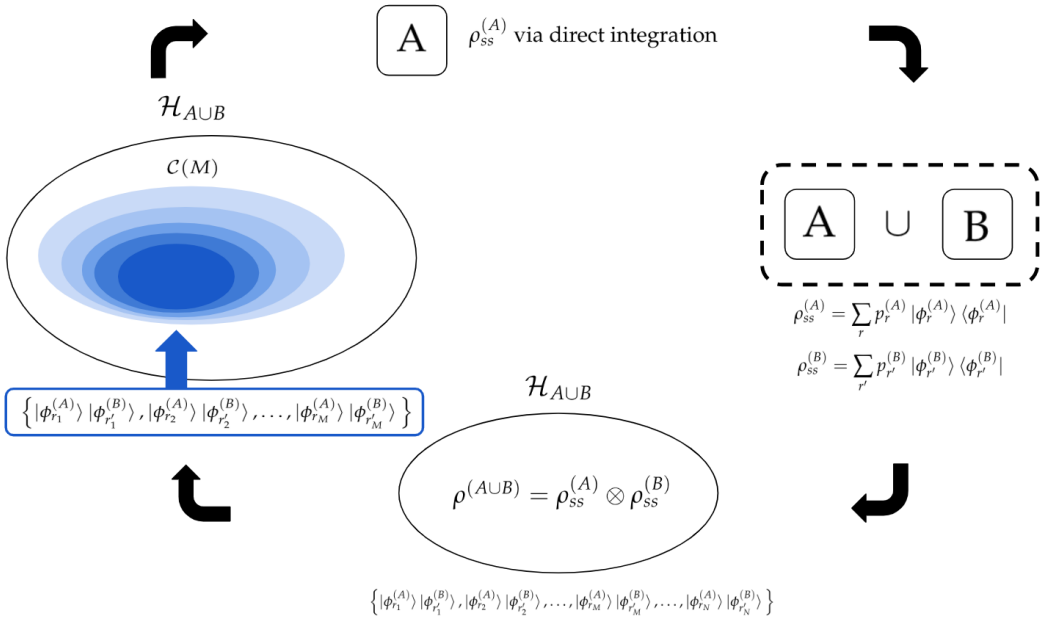


FIGURE 3.3: Sketch of the corner-space renormalization method.

## 3.3 The Matrix Product Density Operators (MPO) Method

Finally, we analyze the *matrix product density operators* (MPO) method. This method is rooted in one of the first and most efficient numerical methods: the *density matrix renormalization group* (DMRG) [53, 54, 45].

Essentially, the DMRG is a generalization of Wilson's NRG method; its core lies in the construction of the so-called *superblock* (see fig. 3.4): it is constructed in an iterative way, taking a portion of the system, then enlarging it until the desired size is reached; this superblock is usually indicated as $A \bullet \bullet B$. By numerical diagonalization of $H_{A\bullet\bullet B}$ one can find the ground state $|\Psi_{GS}\rangle$ that minimize the energy:

$$E = \langle\Psi_{GS}| H_{A\bullet\bullet B} |\Psi_{GS}\rangle .$$

Since we do not want an exponential increase of the dimension of the Hilbert space, we choose the D most relevant states for block $A\bullet$ (similarly for $\bullet B$). So, having the reduced density operator for $A\bullet$:

$$\rho_{A\bullet} = \mathrm{Tr}_{\bullet B} |\Psi_{GS}\rangle \langle\Psi_{GS}| .$$

one uses the D eigenstates with the largest weight (i.e. with the largest eigenvalues) to construct the pseudo-unitary matrix O, useful to truncate the basis:

$$H_{A'} = O H_{A\bullet} O^{\dagger}.$$

At this point, one can replace the first block with the new $A'$.

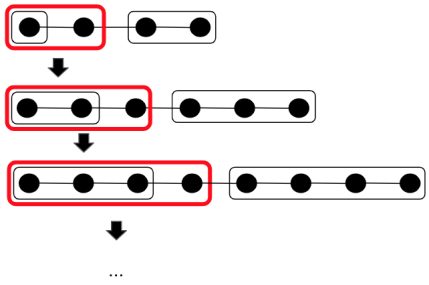

FIGURE 3.4: Sketch of superblocks formation in DMRG method.

The MPO method is the generalization of the *matrix product states* (MPS) method [46], which is useful in the description of (closed) quantum many-body systems. The essential idea [10] behind the MPS techniques lies in Wilson's renormalization group, already mentioned in sec. 3.2. So, let us consider two spins and a subspace of the corresponding Hilbert space $\mathcal{H}_2 \subset \mathcal{H}_1 \otimes \mathcal{H}_1$ of dimension $d_2 \leq d_1^2$; we write an arbitrary orthonormal basis $\{|\beta\rangle\}_{\beta=1}^{d_2}$ as

$$|\beta\rangle_2 = \sum_{n_1,n_2}^{d_1} B_\beta^{n_1,n_2} |n_1\rangle_1 \otimes |n_2\rangle_1 ,$$

where $B_\beta^{n_1,n_2}$ are the coefficients of the basis vectors in terms of the original basis vectors $|n\rangle \in \mathcal{H}_1$ and can be expressed as

$$B_\beta^{n_1,n_2} = \sum_{\alpha=1}^{d} {}_1A[1]_\alpha^{n_1} A[2]_{\alpha,\beta}^{n_2},$$

where $A[1]_\alpha^{n_1} = \delta_{n1,\alpha}$ and $A[2]_{\alpha,\beta}^{n_2} = B_\beta^{\alpha,n_2}$. So, we can now write any orthonormal basis in $\mathcal{H}_3$ in terms of $|\beta\rangle_2 \otimes |n_3\rangle$ and go on iteratively. After M steps, we have:

$$|\beta\rangle_M = \sum_{\alpha=1}^{d_{M-1}} \sum_{n_M=1}^{d_1} A[M]_{\alpha,\beta}^{n_M} |\alpha\rangle_{M-1} \otimes |n_M\rangle_1 ,$$

that is, substituting recursively the definition of $|\alpha\rangle_m$:

$$|\beta\rangle_N = \sum_{n_1,\ldots,n_N=1}^{d_1} (A_1^{n_1} A_2^{n_2} \ldots A_N^{n_N})_\beta |n_1,\ldots,n_N\rangle ,$$

i.e.

$$|\psi_{MPS}\rangle = \sum_{n_1,\ldots,n_N=1}^{d_1} A_1^{n_1} A_2^{n_2} \ldots A_N^{n_N} |n_1,\ldots,n_N\rangle . \tag{3.14}$$

Because of the form of , this vectors are called *matrix product states* (MPS).

For periodic boundary conditions the form of the 3.14 is obtained performing the trace over their product [46, 50]:

$$|\psi_{MPS}\rangle = \sum_{n_1,\ldots,n_N=1}^{d} \mathrm{Tr}(A_1^{n_1} A_2^{n_2} \ldots A_N^{n_N}) |n_1,\ldots,n_N\rangle . \tag{3.15}$$

One should note that the total number of parameters turns out to be $N \times d \times D^2$, i.e. it is linear in $N$.

Another way of considering the expression 3.14 is the graphical notation to represent the operators $A_i^{[k]}$ sketched in figure 3.5. Here, every operator is represented by a square with 3 legs: there are two of them for the bonds with the neighbouring operators, the other one for the physical index.

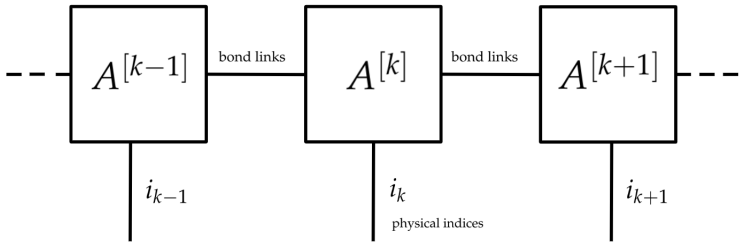


FIGURE 3.5: Graphical representation of an MPS in terms of tensor network.

The matrix product *density operators* (MPO) extend the MPS from pure to mixed states, following the idea explained, for example, in [50]. The physical index is now doubled, as illustrated in fig. 3.6

$$\rho_{MPO} = \sum_{i_1,\ldots,i_N=1}^{d} \sum_{j_1,\ldots,j_N=1}^{d} \mathrm{Tr}\left(A_1^{i_1,j_1}\ldots A_N^{i_N,j_N}\right)|i_1,\ldots,i_N\rangle\langle j_1,\ldots,j_N|\,. \tag{3.16}$$

The $A^{[k]i_k,j_k}$ are $D^2 \times D^2$ tensors that can be decomposed in this way:

$$A_k^{i,j} = \sum_{a=1}^{d_k} M_k^{i,a} \otimes (M_k^{j,a})^*.$$

Also in this case, there is a graphical notation to represent the tensors $A_{i,j}^{[k]}$ sketched in figure 3.6. Here, every tensor is represented by a square with 4 legs: there are two of them for the bonds with the neighbouring tensors, the other two for the physical indices (the "bras" and "kets").

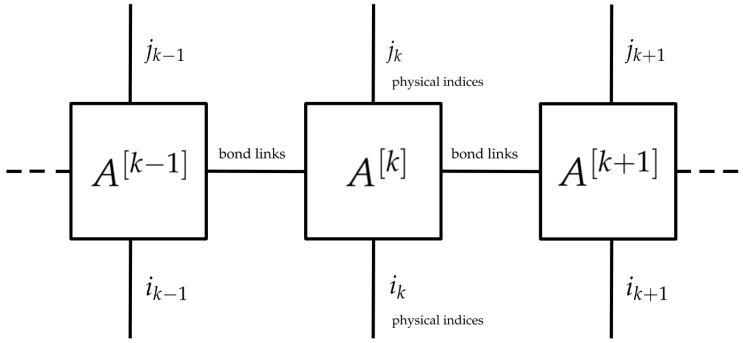


FIGURE 3.6: Graphical representation of an MPO in terms of tensor network.

As regards dynamics, the long-time limit of eq. 3.1 can be reached using a MPO ansatz for the density matrix. The steady-state solution $\rho$ is found using an algorithm based on the *time evolution block decimation* (TEBD) [51] scheme adapted to open systems. It is useful to efficiently compute time-dependent properties of 1D closed quantum many-body systems as done in [52].

Here, we can briefly see how it works [23] in the case of open many-body systems in the MPO formalism.

First of all, let us consider the 3.16: repeated single-value decomposition of the tensor $A^{i_1,\dots,i_N;j_1,\dots,j_N}$ can lead to

$$\rho_{MPO} = \sum_{i_1,\dots,i_N=1}^{d} \sum_{j_1,\dots,j_N=1}^{d} \sum_{\alpha_1,\dots,\alpha_{N-1}=1}^{\chi} (\Gamma^{[1]i_1,j_1}_{1,\alpha_1}\lambda^{[1]}_{\alpha_1})(\Gamma^{[2]i,j_2}_{\alpha_1,\alpha_2}\lambda^{[2]}_{\alpha_2})\dots \times(\lambda^{[N-1]}_{\alpha_{N-1}}\Gamma^{[N]i_N,j_N}_{N,\alpha_{N-1}})||i_1,\dots,i_N,j_1,\dots,j_N\rangle\rangle.$$

where the superoperator formalism[3] is been used in order to write the superket $||i_1,\dots,i_N,j_1,\dots,j_N\rangle\rangle$. The bond-link dimension $\chi$ can be kept under a threshold by discounting the smallest single values; moreover, it is proportional to the amount of quantum correlation between the system sites that can be embedded in $\rho_{MPO}$.

Formally, the solution of 3.1 can be written as

$$\rho(t) = e^{\hat{\mathcal{L}}t}\rho(0). \tag{3.17}$$

Following the Vidal's work [52], the liouvillian superoperator $\hat{\mathcal{L}}$ can be decomposed in this way:

$$\hat{\mathcal{L}} = \hat{F} + \hat{G}, \tag{3.18}$$

where

$$\begin{aligned} \hat{F} &\equiv \sum_{\text{even } l} (\hat{\mathcal{L}}^{l,l+1}) \\ \hat{G} &\equiv \sum_{\text{odd } l} (\hat{\mathcal{L}}^{l,l+1}), \\ l &= 1,\dots N-1 \end{aligned} \tag{3.19}$$

having considered a Liouvillian made of arbitrary nearest-neighbouring interaction terms.

For every small time step $\tau > 0$, the Trotter-Suzuki expansion of order $p$ for $\exp(\hat{\mathcal{L}}t)$ reads:

$$e^{\hat{\mathcal{L}}t} = e^{(\hat{F}+\hat{G})t} = e^{[(\hat{F}+\hat{G})\tau]\frac{t}{\tau}} \approx [f_p(U_{F\tau}, U_{G\tau})]^{\frac{t}{\tau}},$$

where $U_{F\tau} \equiv e^{F\tau}$ and $U_{G\tau} \equiv e^{G\tau}$ and where

$$f_1(x,y) = xy, \quad f_2(x,y) = x^{1/2}yx^{1/2}$$

for the first and the second order expansions. The simulation of time evolution 3.17 can then be accomplished by iteratively applying $U_{F\tau}$ and $U_{G\tau}$ to $\rho(0)$ a number $\mathcal{O}(\frac{t}{\tau})$ of times.

[3] Every linear operator $\hat{A}$ acting on the Hilbert space $\mathcal{H}$ can be associated with a vector in a superoperator space:

$$\hat{A} = \sum_{ij} A_{ij}\,|i\rangle\langle j| \quad \rightarrow \quad |A\rangle\rangle = \sum_{ij} A_{ij}\,|i\rangle|j\rangle\,.$$

# Chapter 4

# Case Study: a 1/2-spin XYZ Heisenberg Chain Coupled to Two External Baths

## 4.1 The Model

Non-equilibrium dynamics of quantum many-body systems have become a subject of great interest, due especially to the breakthrough in the experimental methods in the field of ultracold atoms. As already mentioned in chapter 2, several platforms, which have been theorised or implemented [47], can realize one-dimensional spin chains with great accuracy.

One of the oldest and paradigmatic model of interacting quantum particles is the Heisenberg model. Despite being exactly solvable by the Bethe ansatz, calculating its properties is not trivial.

In the present work, we have chosen to consider the anisotropic Heisenberg model: the Heisenberg XYZ chain of N $\frac{1}{2}$-spin, coupled to two external reservoirs positioned at its boundaries. The density matrix describing the chain evolves according to the Lindblad master equation

$$\frac{d\rho}{dt} = -i[H,\rho] - \sum_{a=1}^{N} \gamma_a \Big( \frac{1}{2} L_a^\dagger L_a \rho + \frac{1}{2} \rho L_a^\dagger L_a - L_a \rho L_a^\dagger \Big), \tag{4.1}$$

where the bath-coupling strength parameters $\gamma_a \neq 0$ only for $a = 1, N$ and $H$ being the Hamiltonian of the model:

$$H = \sum_{i=1}^{N-1} (J_x \sigma_i^x \sigma_{i+1}^x + J_y \sigma_i^y \sigma_{i+1}^y + J_z \sigma_i^z \sigma_{i+1}^z), \tag{4.2}$$

where $\sigma^x$, $\sigma^y$ and $\sigma^z$ are the Pauli matrices, which are defined as follows:

$$\sigma^x = \begin{pmatrix} 0 & 1 \\ 1 & 0 \end{pmatrix}, \quad \sigma^y = \begin{pmatrix} 0 & -i \\ i & 0 \end{pmatrix}, \quad \sigma^z = \begin{pmatrix} 1 & 0 \\ 0 & -1 \end{pmatrix}. \tag{4.3}$$

The coupling constant are choose to be $J_x = 1$, $J_y = 0.5$ all over the dissertation, while $J_z$ will be varied as it will see in the following sections. However, in this chapter it assumes the value $J_z = 1$, when not specified differently. The $L_a$ are the Lindblad operators representing the single-spin bath coupled to the first and the last spin of the chain:

$$L_1 = \frac{1}{2}(\sigma_x + i\sigma_y), \quad L_2 = \frac{1}{2}(\sigma_x - i\sigma_y). \tag{4.4}$$

In the following sections, we will study three fundamental observables for the analysis of a XYZ Heisenberg chain: the magnetization profile, the two-point correlation function, the spin current; in particular, we will examine them in chains of different size: 8, 12, 16 sites.

All fits in the present and in the next chapters are made by [7] with Minuit/Migrad and Linear minimizers.

## 4.2 Magnetization Profile

The first observable we want examine is the magnetization profile of the chain, i.e. the expectation value $\langle \sigma^z \rangle$ of the Pauli matrix $\sigma^z$ for each site:

$$\langle \sigma^z \rangle = \mathrm{Tr}(\sigma^z \rho_s),$$

being $\rho_s$ the steady-state density matrix of the system.

The magnetization profile is the first marker of the dynamics of the chain: it reveals the behaviour of the system; in particular, it allows us to see the effects generated by the presence of the dissipators, described by the Lindblad operators 4.4. One should expect the profile to have the ends polarized toward opposite directions, because of the position (in the first and in the last chain site) of the dissipators.

The behaviour of magnetization is shown in fig. 4.1; it is congruent with the reasoning made before. The profile is symmetrical in respect to the center of the chain, while the first half is characterized by positive values of $\langle \sigma^z \rangle$ and the second half by negative values of $\langle \sigma^z \rangle$, because the first dissipator (positioned in the first site) forces spins to align along the positive z-axis. The opposite happens for the second dissipator.

Moreover, in order to make sure the numerical results are under control, a comparison between MPO and QT methods is done for a 8-sites chain. It is clear that the results are overlapping, so it is reasonable to treat them as plausible ones.

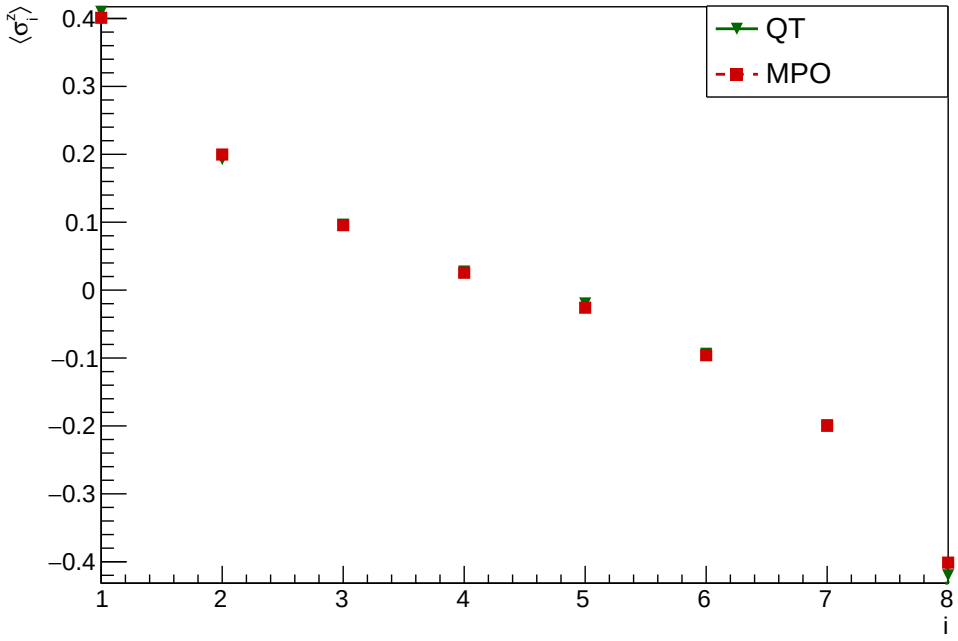


FIGURE 4.1: Spin profile for a 8-sites chain characterized by $\gamma = 1$, $J_x = 1$, $J_y = 1$, $J_z = 1$; $i$ stands for the site index.

Now, it is interesting to investigate how the change of chain length modifies the magnetization profile. In fig. 4.2 it is shown the comparison between the magnetization profile of chains with different lengths. Two characteristics stand out: the first one is the fact that the peak values of $\langle \sigma^z \rangle$ in the ends of the chain are independent from the size of the system; this is true also for different values of $\gamma$: the peak values still remains the same for different lengths of the chain; the second one involves the fact that increasing the length of the chain, the spin profile gets flatter.

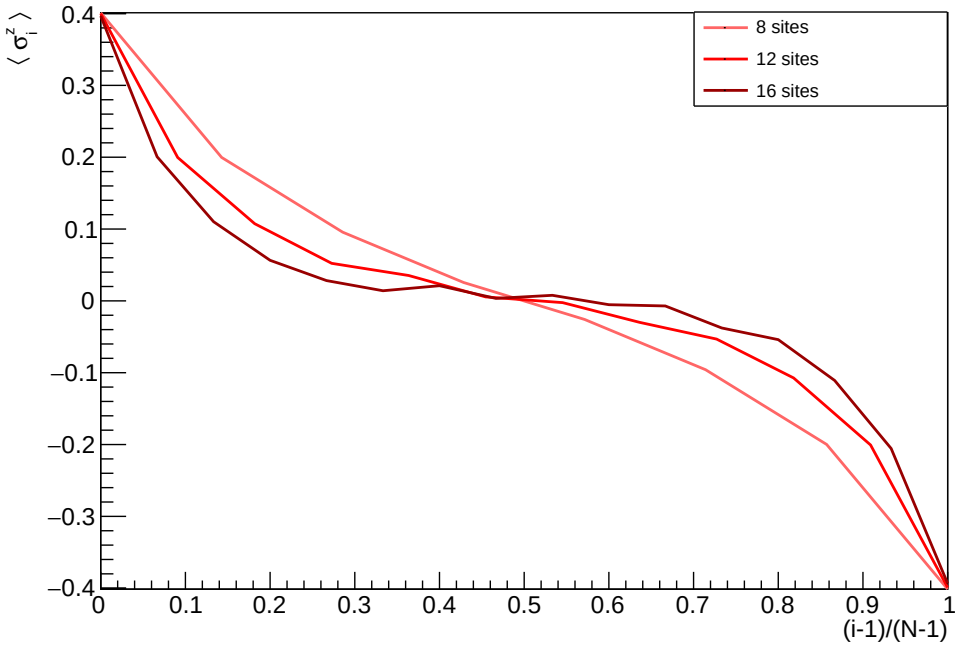


FIGURE 4.2: Spin profile for the model under study at $J_z = 1$ and $\gamma = 1$. Data for different chain length are shown and they are obtained from MPO method.

In order to analyze these properties in more detail, in the following figures we see how the behaviour of magnetization profile changes for different values of dissipation rate $\gamma$.

First of all, it is convenient separate the curves for each size (8, 12 and 16 sites) in order to distinguish the profiles. The plots are shown in figures 4.3, 4.4, 4.5.

It is worth noting several aspects that arise from these plots. First of all, it seems clear that, while increasing $\gamma$, the ends of the chain become more and more polarized. This is true for every length of the chain because, as mentioned previously, the peak values are independent of the length of the chain.

The profile is not trivially linear, but changes while $\gamma$ changes. This trend becomes more and more evident as the length increases. Indeed, while $L$ grows, the plots show with increasing clearness the formation of a *plateau* in which the magnetization is zero. Only near the edges it tends to boost, because of the driving effect of the dissipators.

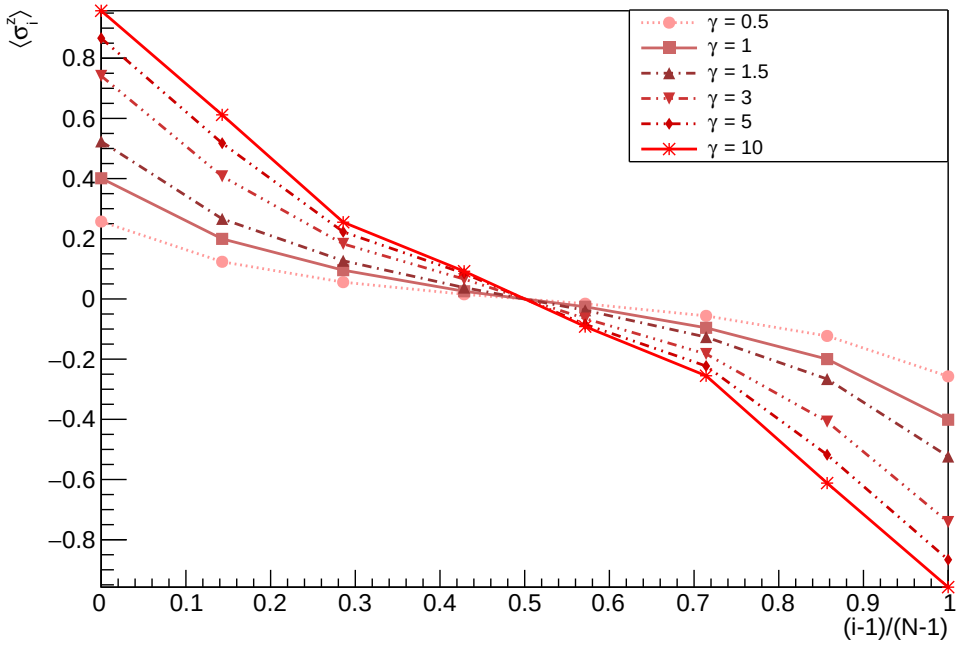


FIGURE 4.3: Spin profile for a 8-sites chain varying on dissipation rate $\gamma$. Data are obtained from MPO method.

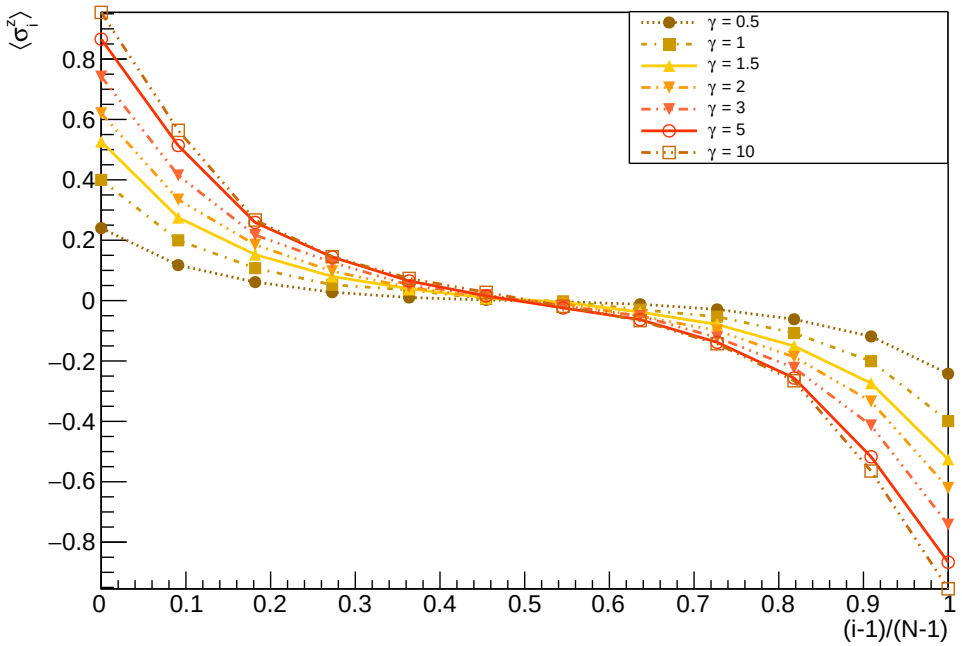


FIGURE 4.4: Spin profile for a 12-sites chain varying on dissipation rate $\gamma$. Data are obtained from MPO method.

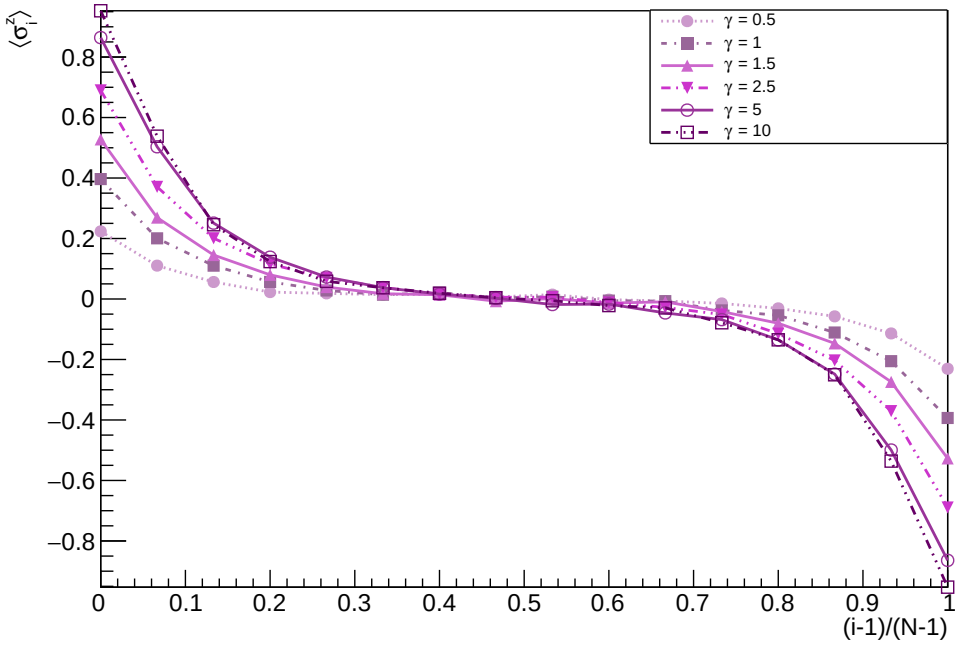


FIGURE 4.5: Spin profile for a 16-sites chain varying on dissipation rate $\gamma$. Data are obtained from MPO method.

As said previously, the peak value of $\langle\sigma^z\rangle$ varies with $\gamma$. In the fig. 4.6 it is presented the fit [7] that shows an exponential behaviour.

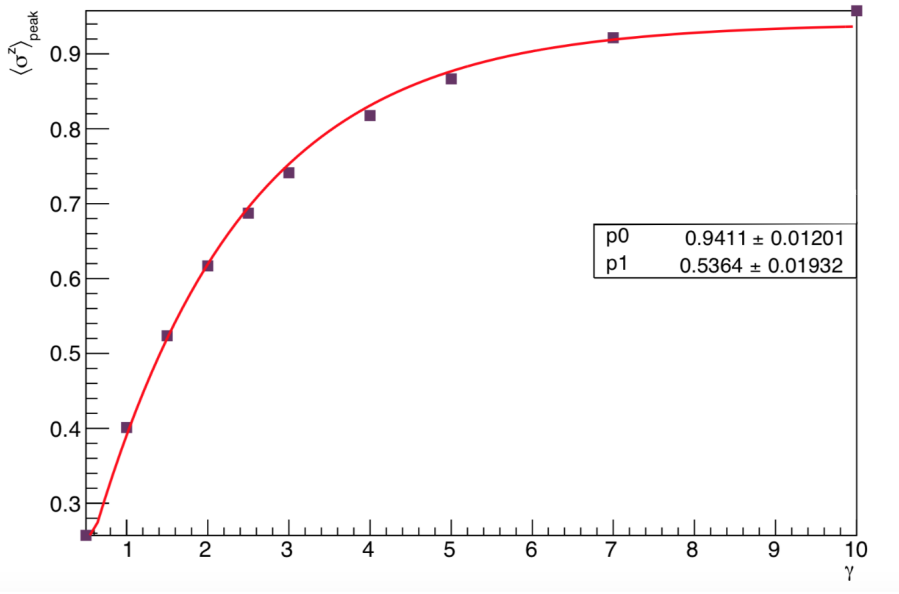


FIGURE 4.6: The red line shows the fit $\langle\sigma^z\rangle_{max} = p_0(1 - e^{-p_1\gamma})$.

It is interesting noting that the same dependence is keep also by $\langle\sigma^z\rangle$ of spins lying in the $\frac{L}{4}$-th site, as shown in fig. 4.7 (the same trend is confirmed in the case of 8 and 12 sites, shown in appendix?).

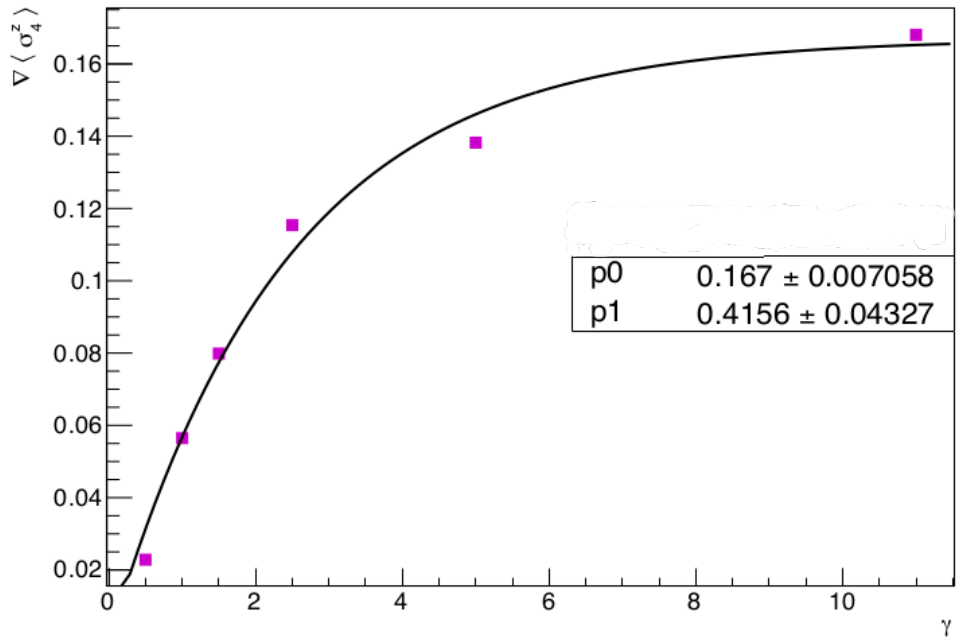


FIGURE 4.7: 16 sites, the black line shows the fit $\langle\sigma^z_{4th}\rangle(\gamma) = p_0(1 - e^{-p_1\gamma})$. textcolorredError in the label of y-axis.

These two plots displayed in fig. 4.6 and in fig. 4.7 show that for large values of $\gamma$, i.e. for more and more important driving, $\langle\sigma^z\rangle$ tends asymptotically to a maximum value.

## 4.3 Two-Points Correlation Functions

Another observable of interest is certainly the steady-state two-point correlation function, defined as follows:

$$C(i,j) = \langle\sigma_i^z\sigma_j^z\rangle - \langle\sigma_i^z\rangle\langle\sigma_j^z\rangle, \tag{4.5}$$

where $\langle\sigma_i^z\sigma_j^z\rangle = \mathrm{Tr}(\sigma_i^z\sigma_j^z\rho_s)$ and $\langle\sigma_i^z\rangle = \mathrm{Tr}(\sigma_i^z\rho_s)$, being $\rho_s$ the steady-state density matrix.

In particular, the two-point correlation function will be studied considering the system symmetry, using the so-called *bulk* correlation function; that is, starting from the middle sites of the chain, the correlation function will be calculated between equidistant sites from the center of the chain.

In the fig. 4.8, 4.9, 4.10 the bulk correlation function for several values of $\gamma$ is shown, for 8, 12 and 16 sites spin chain respectively. An interesting aspect that is quite clear in these plots, involves the finite-size effect; while the size of the chain grows, the exponential profile of the correlation function become more clear. Indeed, only starting from size of 12 sites the exponential profile starts to stand out.

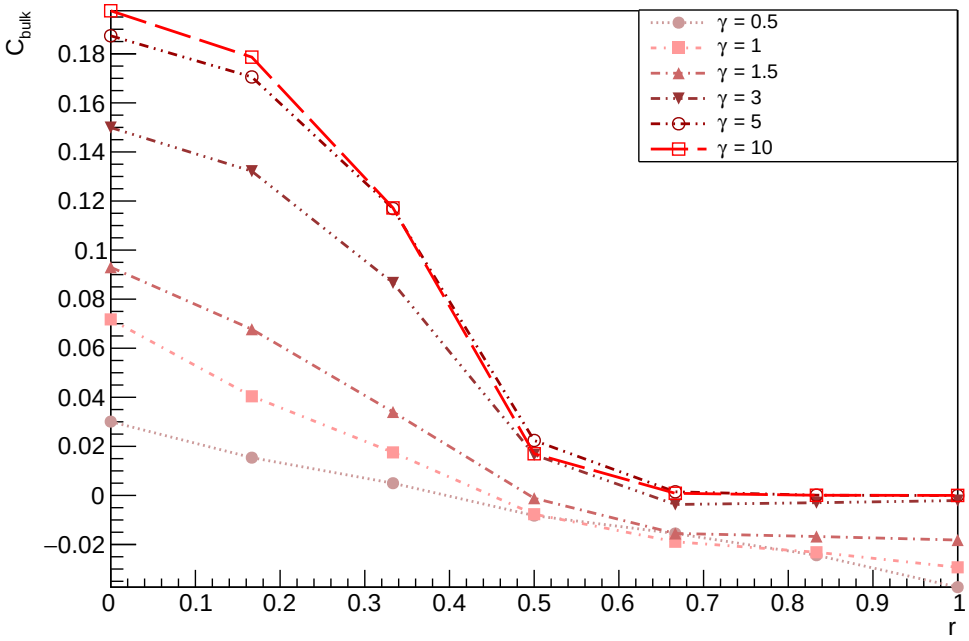


FIGURE 4.8: Bulk correlation function for a 8-sites spin chain. Data are obtained from MPO method.

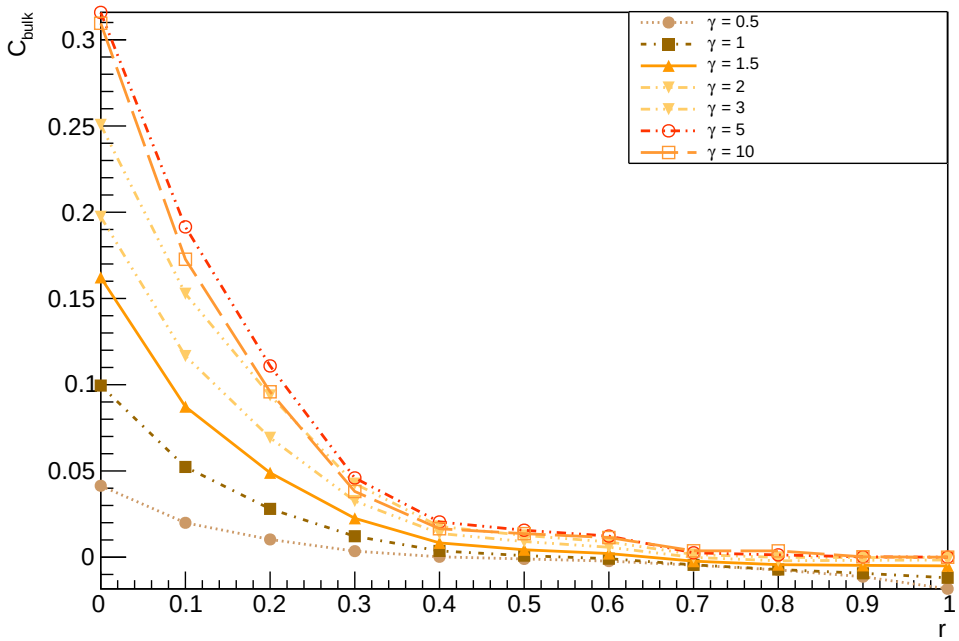


FIGURE 4.9: Bulk correlation function for a 12-sites spin chain. Data are obtained from MPO method.

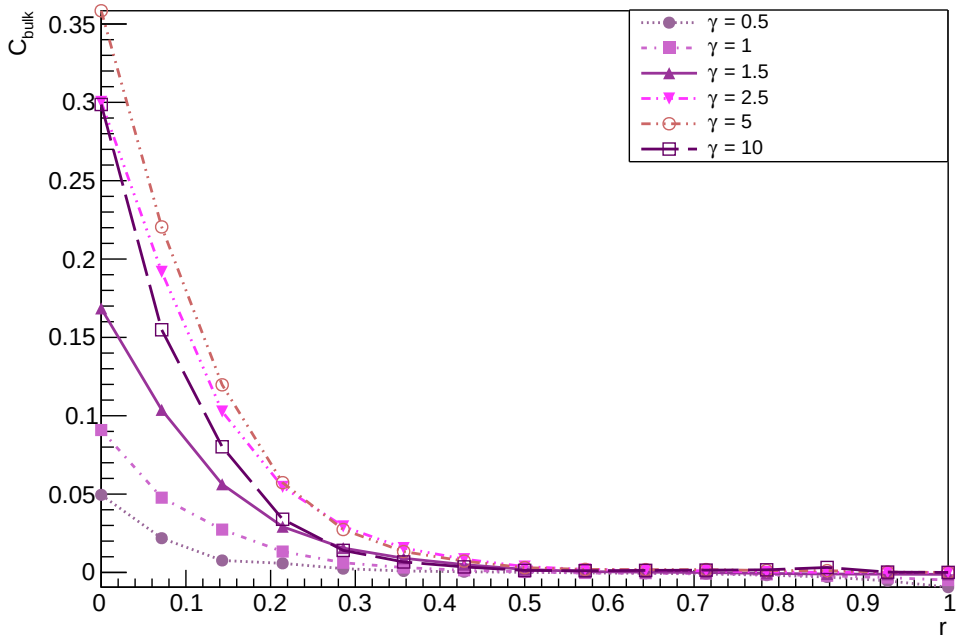


FIGURE 4.10: Bulk correlation function for a 16-sites spin chain. Data are obtained from MPO method.

The fit made with [7] shows that the profile of correlation function is exponential. In fig. 4.11 several observations can be made; first of all, the trend of the two-point correlation function is exponential. In particular, the dependence from the distance between the spin reads:

$$C(r) = p_0 e^{-p_1 r},$$

where the coefficients $p_0$ and $p_1$ are given by the fit and are displayed in fig. 4.11. Here, we can see that the correlation between nearest neighbours (i.e. the first point of every curve) gets bigger as $\gamma$ grows.

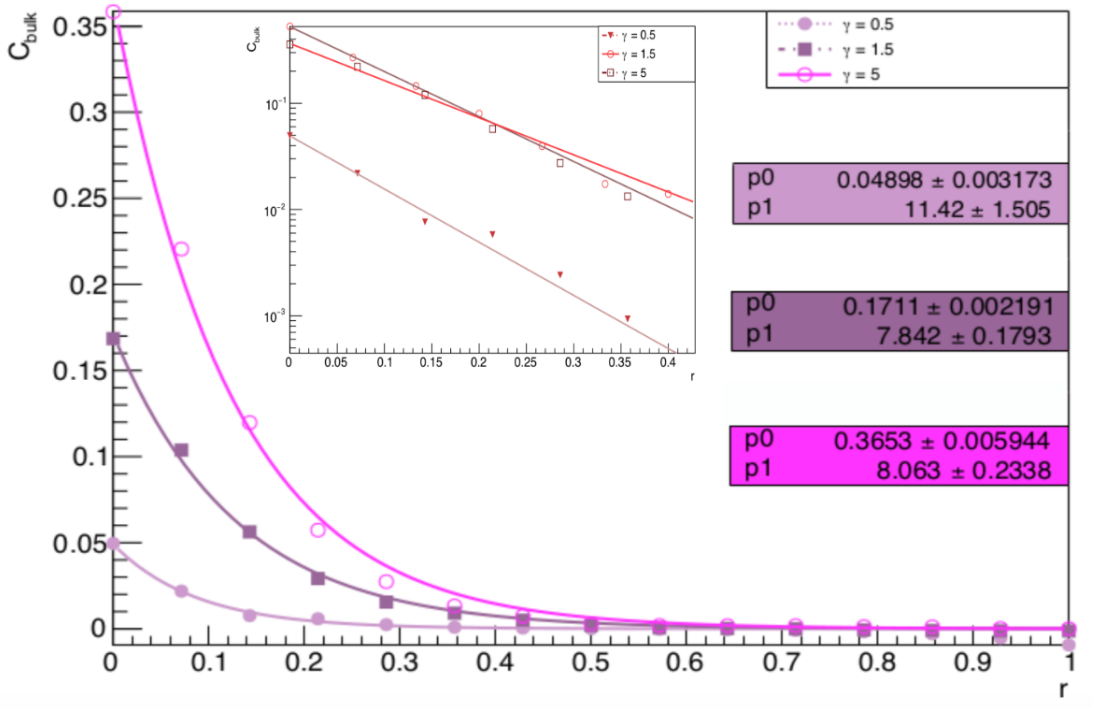


FIGURE 4.11: Bulk correlation function for a 16-sites spin chain for several values of $\gamma$. It is shown the fit $C_{\text{bulk}} = p_0 \exp(-p_1 r)$. The fit parameters are show in the same order of the legend for $\gamma$. In the box there is the same fit in a semi-logarithmic scale.

## 4.4 Spin Transport

In this section we are going to study the spin current $j_\sigma$ defined from the continuity equation for the local spin operators [3]:

$$\frac{\partial S_z^k}{\partial t} + \nabla (j_\sigma)_k = 0, \tag{4.6}$$

which can be rewritten as

$$(j_\sigma)_{k+1} - (j_\sigma)_k = \frac{i}{2}[\sigma_k^z, H], \tag{4.7}$$

where $S_k^z \equiv \sigma_k^z/2$ and where $H$ is the Hamiltonian written in 4.2. So, we obtain:

$$j_\sigma = J_y(\sigma_k^x \sigma_{k+1}^y) - J_x(\sigma_k^y \sigma_{k+1}^x). \tag{4.8}$$

As done previously for the observables already studied, we can see how the spin current changes for chain of different lengths with the same model. In fig. 4.12 it is shown the spin current for a 8, 12 and 16-sites chain, characterized by $J_z = 1$ and dissipation rate $\gamma = 1$. The curves are asymmetric, due to the fact that the Heisenberg model XYZ has an intrinsic anisotropy. While the length of the chain increases, the spin current shows a flatter profile which is consistent with the fig. 4.2 where the plateau of null magnetization becomes bigger while the size of the chain grows.

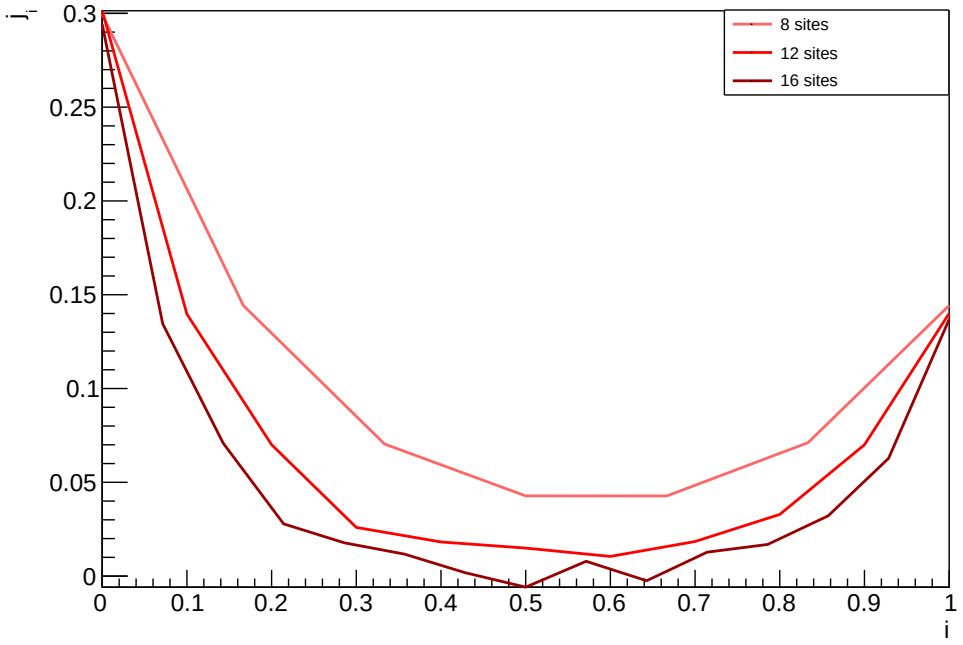


FIGURE 4.12: Spin current for the model at $J_z = 1$. Data for different chain lengths are shown. They are obtained from MPO method.

An aspect worth considering is the common peak value of the spin current, independent of the chain size. As done in the section 4.2 studying the magnetization profile, we can see how this value changes varying $\gamma$.

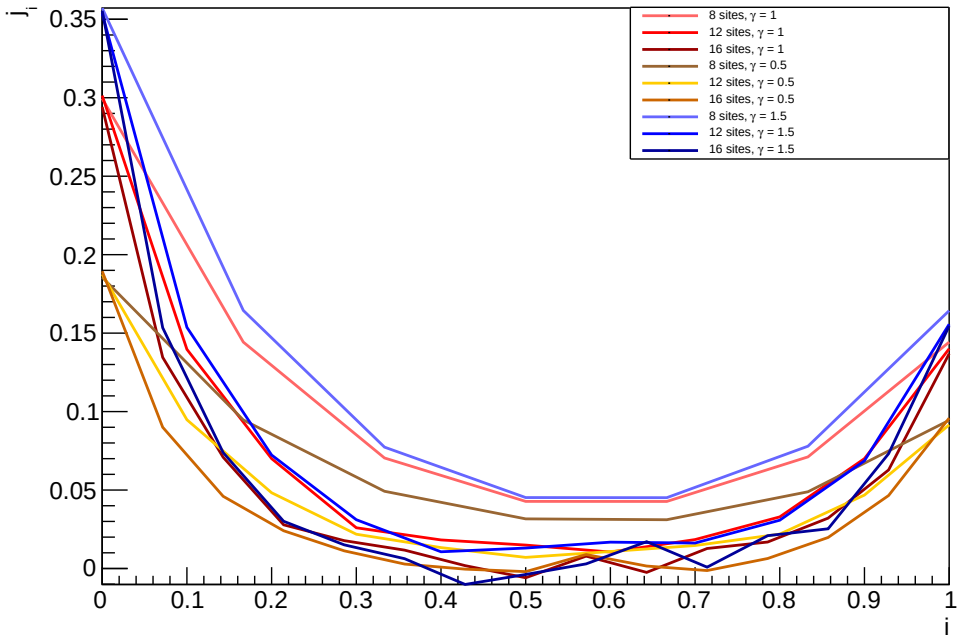


FIGURE 4.13: Spin current for the model at fixed $J_z = 1$, for several values of $\gamma$.

It is interesting noting that the peak values reach a maximum and then decrease, as shown in fig. 4.14. This can be explained analyzing the curve. First of all, for small values (i.e. $\gamma \sim 0.5$) there is a non-null spin current; as said, for a certain value of $\gamma$ the spin current reaches the maximum value and then begins to decrease tending asymptotically to zero. While $\gamma$ grows, the dissipation acquires a more important role over the Hamiltonian dynamics, the system is driven so that its spin current is zero. This is consistent with the trend shown in fig. 4.6 of the positive peak value of $\langle \sigma^z \rangle$ and in fig. 4.7 of the value of $\langle \sigma^z \rangle$ for the forth site of the chain, in which while $\gamma$ increases the magnetization tends asymptotically to a constant value.

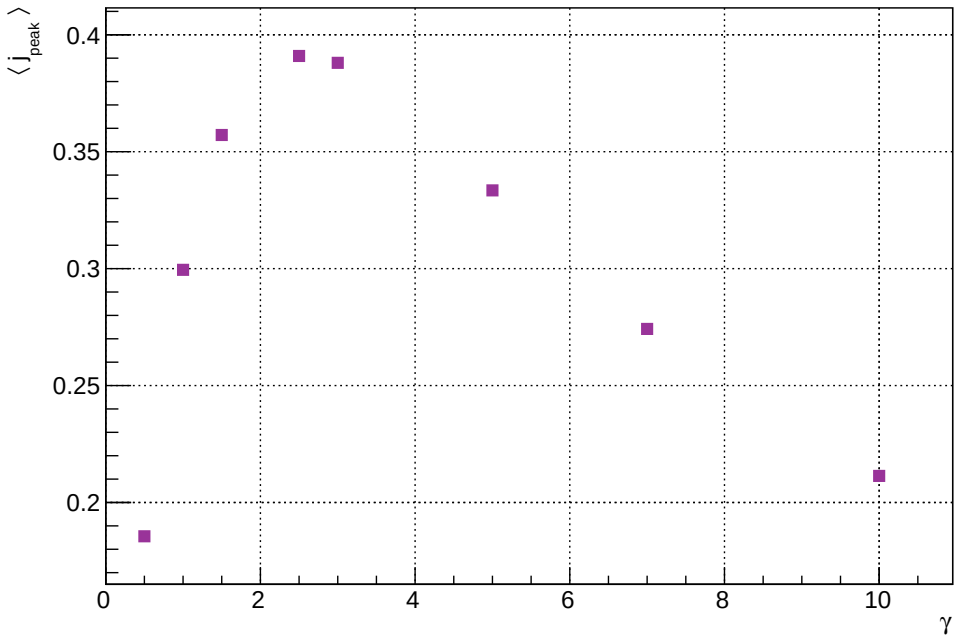


FIGURE 4.14: Peak values of spin current for several values of $\gamma$. Data are obtained from MPO method.

## 4.5 The CSR Method: Limitations and Usability

The CSR method, described in section 3.2, has been studied and implemented in order to analyze the model described in the last section. The algorithm is written in pseudocode in appendix A.

In this section, it is shown that the CSR method is not a suitable method for investigating systems described by a model such as the one under consideration.

In order to reveal this, we can easily see the case of a 4-sites chain for the proposed model. In particular, we can study the magnetization profile of the chain, i.e. the steady-state expectation value $\langle \sigma^z \rangle$ of the Pauli spin- matrix $\sigma^z$ for each site:

$$\langle \sigma^z \rangle = \mathrm{Tr}(\sigma^z \rho),$$

being $\rho$ the steady-state density matrix of the system.

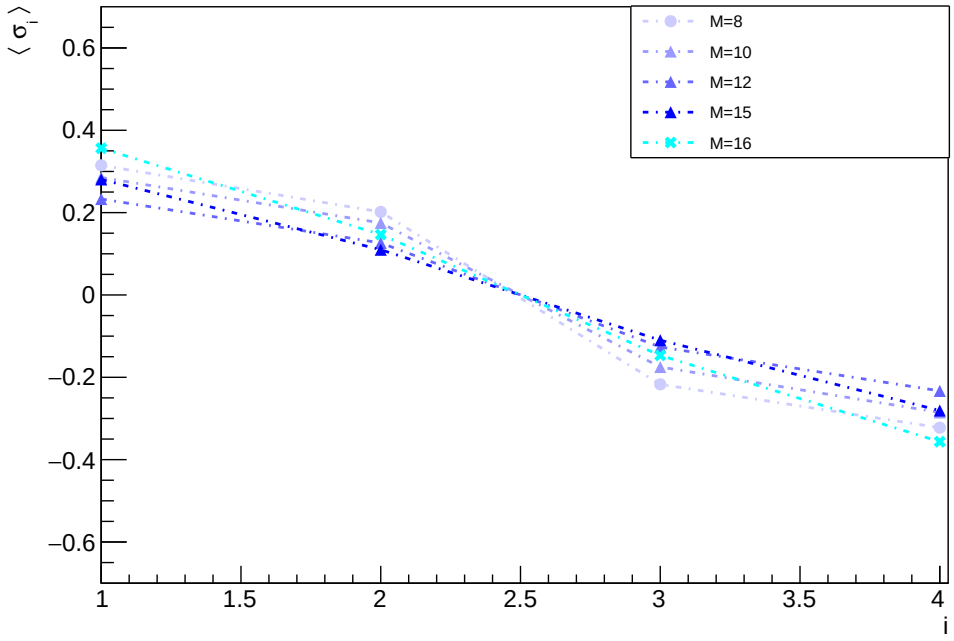


FIGURE 4.15: Spin profile of a 4-sites chain for the model described above with $J_z = 1$ for several values of corner-space dimensions $M \times M$. The cyan markers are those representing the expectation value of the magnetization calculated by means of a complete set of states of Hilbert space (which has dimension $2^4$).

As shown in figure 4.15, it is clear that for such a system the convergence has not been reached. Even for $M = 15$, that covers almost the total Hilbert space dimension, the results are not the convergent ones.

On the other hand, if we consider a model in which every site is coupled to a dissipator, we can see how the magnetization profile gets to convergence starting from $M = 9$ already.

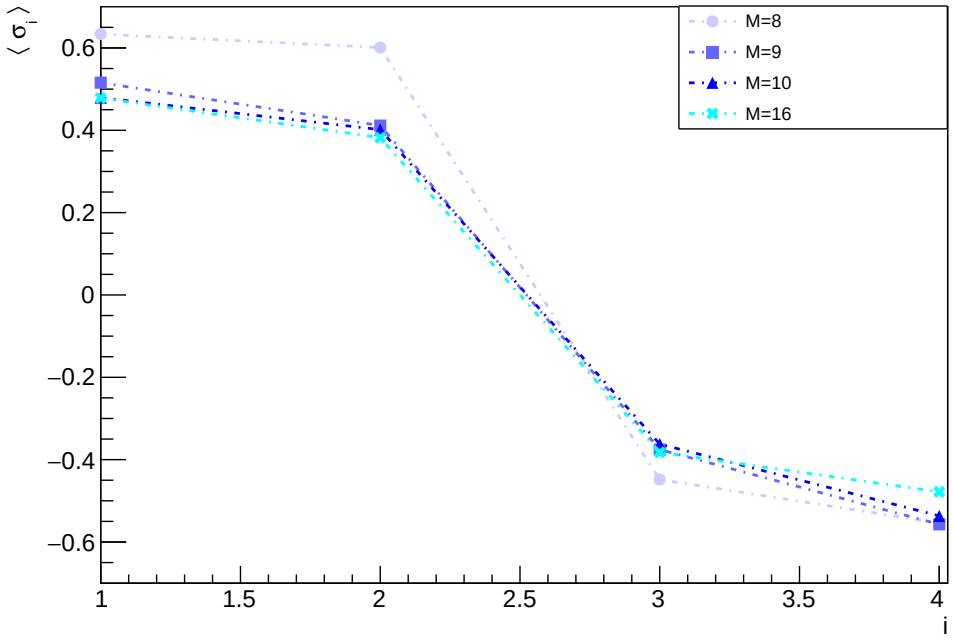


FIGURE 4.16: Spin profile of a 4-sites chain in which every spin of the chain is coupled to a dissipator. In this case, the convergence is reached for $M < \dim(\mathcal{H})$.

In order to confirm the limitations of this method, the same comparison is done for a longer chain, made up by 8 sites. In this case, the results of CSR method are compared to those of MPO method, since a brute-force diagonalization of the Liouvillian operator would not be possible: it would require a huge amount of memory. We have reason to believe that the results obtained from MPO method are plausible, as we will see in the next sections.

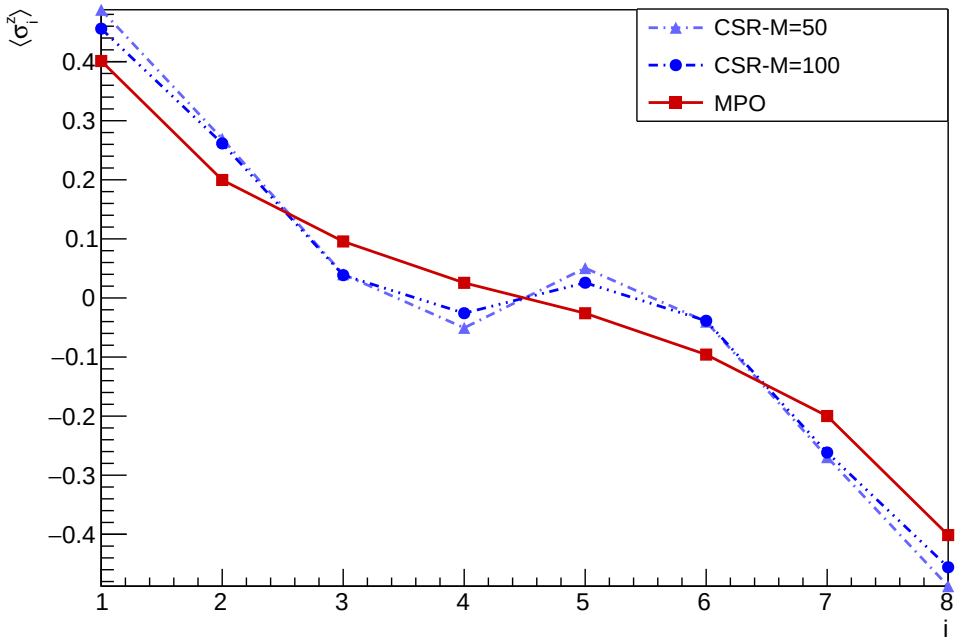


FIGURE 4.17: Spin profile of a 8-sites chain for the model described in sec.4.1. Significant differences between the data obtained for $M = 50$ and $M = 100$ are not noticed.

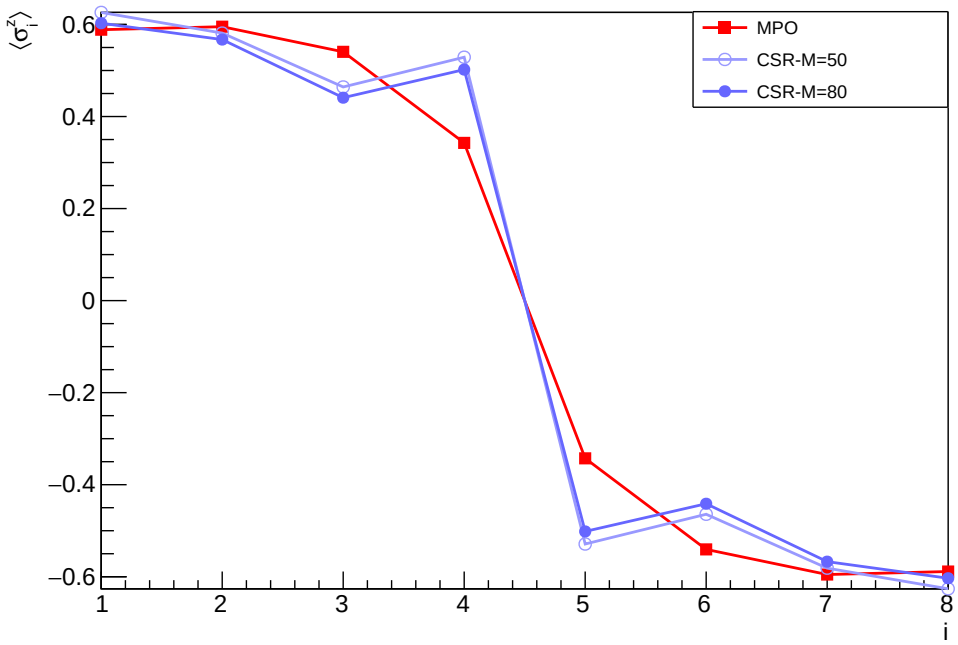


FIGURE 4.18: Spin profile of a 8-sites chain in which every spin of the chain is coupled to a dissipator.

In conclusion, in fig. 4.20 it is displayed the magnetization profile of a 16-sites chain obtained by CSR and MPO methods.

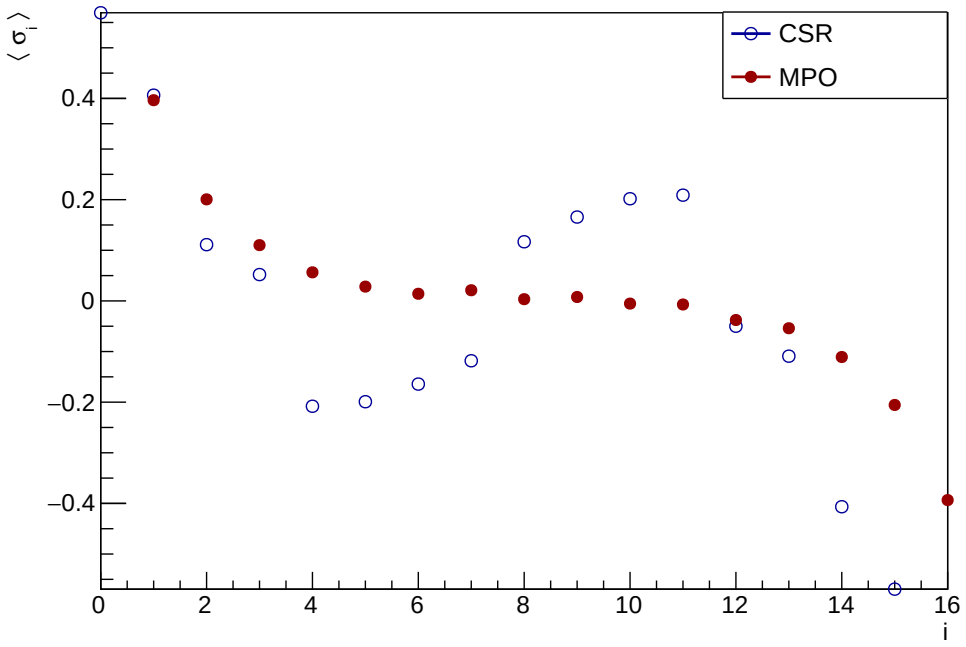


FIGURE 4.19: Spin profile for a 16-sites chain for the model described in section 4.1. Data in red are obtained from MPO method, with m = 80 and T = 2000 and data in blue are obtained from CSR method, with M = 65. It is self-evident the inadequacy of the corner-space method, for the model under study.

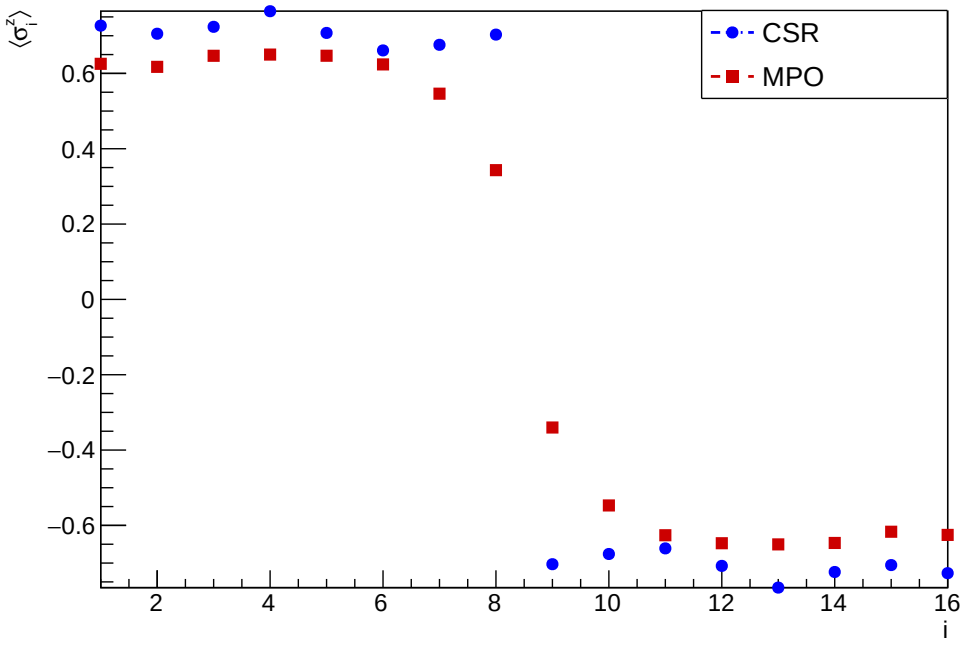


FIGURE 4.20: Spin profile for a 16-sites chain in which every spin of the chain is coupled to a dissipator. The dimension of the corner-space is $M = 65$.

# Chapter 5

# A Nonequilibrium Phase Transition

In an open system, the competition between unitary Hamiltonian evolution and dissipation can induce a dissipative phase transition for the steady state, as discussed for example in the case of spin systems by [25]. A phase transition is an important phenomenon in condensed-matter physics and can happens tuning one or more parameters of the Hamiltonian of the system.

So far, we have studied the behaviour of 8, 12 and 16-sites chain varying the coefficient of dissipation rate $\gamma$. In this chapter, the behaviour of the chains under a variation of $J_z$ will be investigated.

First of all, we have analyzed the spin current under the variation of the coupling constant $J_z$. In fig. 5.1 the spin current for several values of $J_z$ is displayed. Some consideration can be made in regards to this plots.

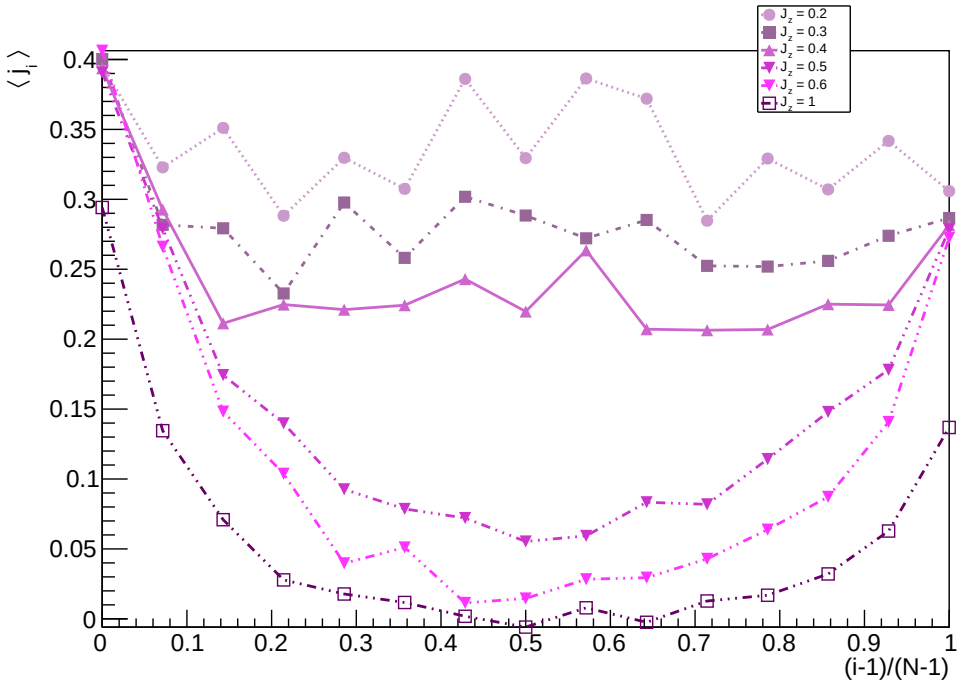


FIGURE 5.1: Spin current of a 16-sites chain, with $\gamma = 1$ for several values of $J_z$. Data obtained from MPO method.

The spin current between the first and the last two sites is independent from $J_z$, for $J_z < 1$; this can be a sign of the prevalence of dissipation over the Hamiltonian dynamics. Otherwise, for $J_z \geq 1$ the peak values (i.e. the spin current between the

first two and the last two sites of the chain) drop while $J_z$ increases; this can be a sign of the growing prevalence of the Hamiltonian over the dissipation, while the coupling $J_z$ grows.

For the small values of $J_z$, i.e. for $J_z < 0.5$, the $\sigma_i^z \sigma_{i+1}^z$ term acts as a perturbation of the XY model. For this values, the spin current shows a discontinuous behaviour: the trend of spin current in the middle sites (i.e. all the sites excluding the first and the last) is almost constant. This is an additional sign of the prevalence of the role of dissipation.

For values of $J_z \geq 0.5$, the trend of the spin current is polynomial, with smooth decrease and increase nearby the ends of the chain; while $J_z$ grows, in the middle sites the spin current is more and more constant, sign of the fact that the role of Hamiltonian is more and more predominant.

This irregular behaviour is suggestive of a phase transition; in order to get some numerical evidence of it, we have analyzed also the magnetization profile and the correlation function.

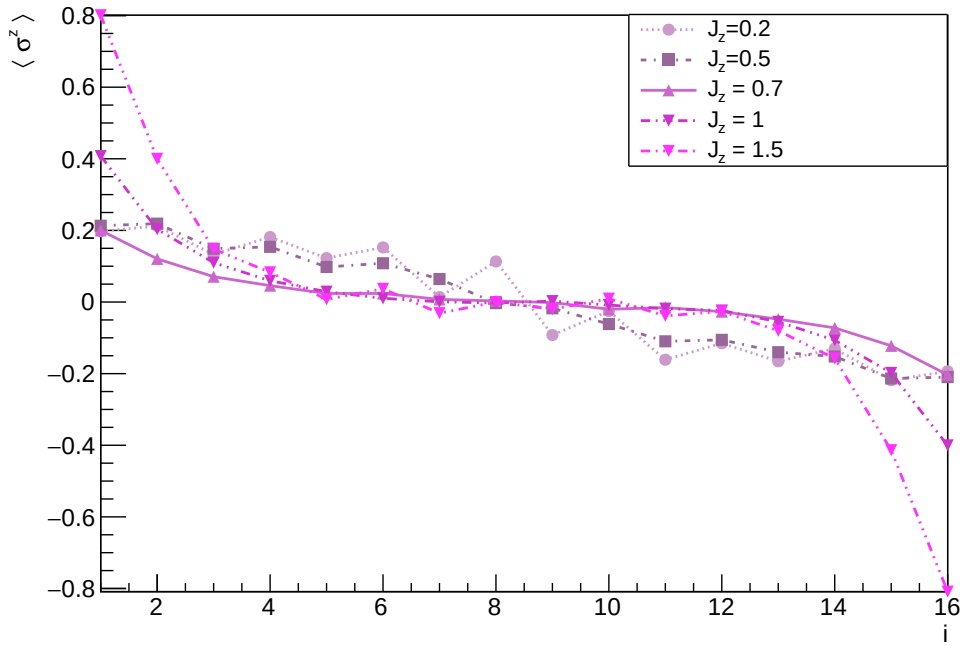


FIGURE 5.2: Magnetization profile of a 16-sites chain, with $\gamma = 1$ for several values of $J_z$. Data obtained from MPO method.

The magnetization profile (displayed in fig. 5.2) for $J_z \geq 1$ shows a similar behaviour to the one seen in the previous chapter, when we considered variation of $\gamma$: the variation of the coupling constant $J_z$ has a similar effect of the one caused by the variation of the dissipation rate $\gamma$.

For small values of $J_z$, i.e. $J_z < 1$, a couple of things can be noted. First of all, for all the $J_z < 1$ the $\langle \sigma^z \rangle$ of the first and of the last spin of the chain is constant. This can be explained as an unimportance of the Hamiltonian terms in relation to dissipation.

It is worth noting that in the magnetization profile does not arise the discontinuity noticed in the trend of the spin current, for $J_z < 0.5$. Analyzing the two-point correlation function can be helpful in order to brighten this hypothesis.

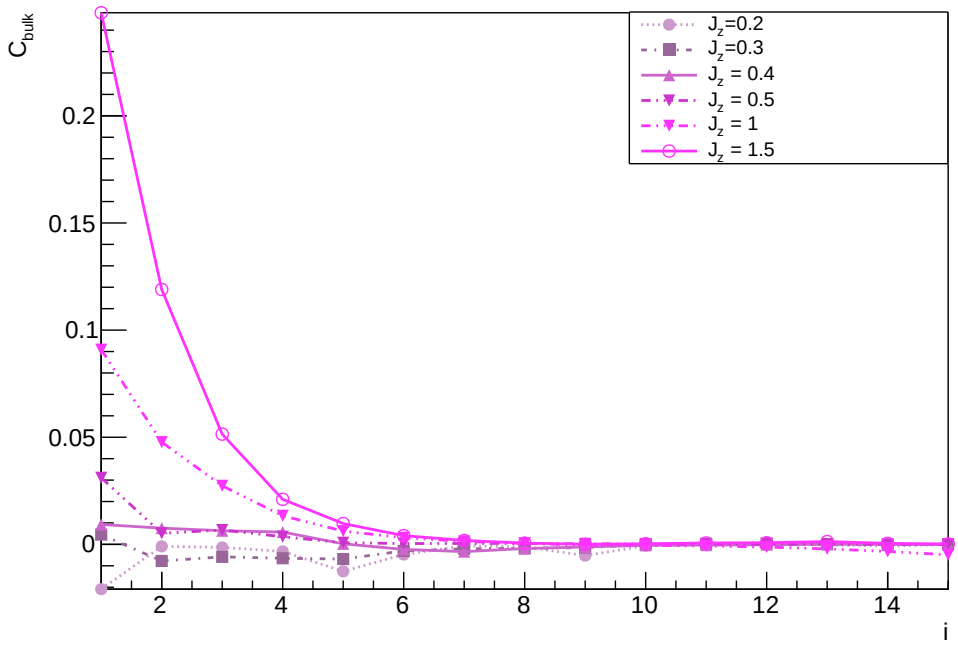


FIGURE 5.3: Correlation function of a 16-sites chain, with $\gamma = 1$ for several values of $J_z$. Data obtained from MPO method.

The two-point correlation function, displayed in fig. 5.3, for $J_z \geq 0.5$ shows a behaviour similar to that seen in the previous chapter, with an exponential profile of the correlation function. In this case, however, there is a discontinuity in its behaviour for $J_z < 0.5$. Indeed, the plots show a null correlation function for such values of $J_z$, trend that is consistent with the profile of spin current in fig. 5.1.

# Conclusions

In the presented work, we have focused on the study of strong correlated quantum systems driven on the edge by quantum baths.

One could wonder why it would be interesting study such a system: the answer comes from the breakthroughs in experimental methods, e.g. in the field of ultracold atoms and QED cavities, the platforms that make it possible to reproduce Hamiltonian models not analyzeable otherwise and consequently to understand complex quantum-physical phenomena.

In the work developed in the previous pages, we have concentrated upon a model, in particular: an anisotropic XYZ Heisenberg spin-1/2 chain driven far from equilibrium with a pair of dissipators acting on the edge of the chain only.

In such a system two kind of dynamics compete: the Hamiltonian one and the dissipative one. We have studied the steady-state to which the system tends while these two dynamics act; in this state, we have analyzed three observables under different regimes of dissipation and of Hamiltonian evolution: magnetization profile, two-point correlation function, spin current.

With regard to magnetization, we have obtained a non-linear trend that becomes more and more clear as the size of the chain increases. In the 16-sites chain, the longest we have studied, the middle part is characterized by zero magnetization and only in the edges it tends to increase; that is plausible because the driving effects prevail in that part of the chain. Moreover, while the dimension of the chain increases the plateau with zero magnetization grows.

The two point correlation function, studied between equidistant spin from the center of the chain, reveals an exponential profile. Here, as in the analysis of the previous observable, the behaviour becomes more evident as the chain dimensions get bigger, because of the size effect.

The third physical quantity that we have examined is the spin current. The profile is polynomial, with two peak values corresponding to the currents between the first two and the last two spin of the chain: they are the maximum values because of the driving effects of the dissipators. From the edge values of spin current, it smoothly decreases. The middle area in which it reach the lowest values gets much flatter as the chain length grows. An interesting thing about the peak values of the spin current is the fact that they reach a maximum value while $\gamma$ increases and then decrease until they asymptotically tend to zero.

Studying the spin current varying the coupling constant $J_z$, we discover a discontinuous behaviour when $J_z < 0.5$: instead of polynomial profile seen varying $\gamma$ (replayed by the spin current of the chain characterized by $J_z \geq 0.5$), the middle spins (i.e. all of them excluding the first and the last) seem to produce a constant current, while in the edges is registered the same spin current for all the chains with $J_z < 1$. A similar behaviour is observed in the study of magnetization profile: the edges of the chain are characterized by the same values for all the values of $J_z < 1$. Here there is no sign of the discontinuity noticed during the study of spin current. Instead, the two-point correlation function reveals another discontinuity again for

$J_z < 0.5$. In particular, for all chains characterized by these values of coupling constant the two-point correlation function is zero.

In order to develop this analysis studying three numerical methods has been necessary. The fundamental use of MPO method, the code of which is not part of the present original work, has allowed us to compute the physical quantities for all lengths of the chain examined in this thesis (8, 12, 16 sites). The QT method has been useful to compare the results obtained from MPO for 8-sites chain and to explore the plausibility of some results for 10-sites chain (here not reported). The CSR method has been studied and implemented but it seems not to be useful for this kind of quantum systems. In particular, it seems to work more properly when all the spins of the chain are coupled to dissipators. For the last two numerical methods, a code has been written and implemented.

# Appendix A

# The Corner-Space Renormalization Algorithm

The purpose of this section is to analyze the code based on the corner-space renormalization algorithm [14] explained in section 3.2.

The code has been written in C++, language useful in this work especially because of the possibility of implementing an object-oriented programming, and employs *Armadillo* [43, 44] as linear algebra library.

**Algorithm 1:** The CSR algorithm for 1D translation invariant systems.

**Input:**

$\mathbf{n}_s$ is the number of sites;

$\mathbf{N}_{iter}$ is the number of iteration necessary to construct the entire system, i.e. $N_{iter} = log_2 n_s$ in the case of a spin-$\frac{1}{2}$ systems;

**M** is the dimension of the corner-space;

**H** is the Hamiltonian of the system;

**for** $i = 1 \rightarrow N_{iter}$ **do**
  determine the steady-state density matrices of two spatially-adjacent blocks
  express the density matrices in terms of an orthonormal basis
  **if** *there is degeneration among eigenvalues* **then**
    apply Gram-Schmidt orthonormalization process
  **else**
    use the basis formed by the eigenvectors of the density matrices
  **end if**
  merge the two density matrices
  express the merged density matrix in terms of an orthonormal basis
  get the pseudo-orthogonal matrix formed by the $M$ most probable product states
  **if** $M >$ *Hilbert space dimension* **then**
    the loop restarts
  **else**
    do the change of basis
  **end if**
  the (new) merged block replaces the old ones
**end for**

One should notice the usefulness of object-oriented programming in the work of turning this algorithm in code. Indeed, the pseudocode written above is actually useful only if the physical system under consideration is invariant under translations, i.e. the merging blocks are the same. In most cases (as that ones considered in chapter 4) there are no symmetries; for dealing with these circumstances, the creation of classes is a great support.

In particular, two classes have been created:

- a **SITE** class: an object of this class has the essential property of the presence (or the absence) of a dissipator, which is characterized by a certain kind of it, e.g. a ladder operator (raising or lowering);
- a **BLOCK** class: a *block* is an object made up by a certain number of objects *site* (you can say it is a nested class). Every time a merge between two blocks is done, a new block emerges. It is characterized by the spatial position: in a merge it is important to know if it is a left or a right block.

In the algorithm 2, a more general version of the code is proposed; the presence of the objects mentioned above allows to treat systems that do not show any symmetry.

**Algorithm 2:** The CSR algorithm for 1D systems.

**Input:**

$\mathbf{n}_s$ is the number of sites;

$\mathbf{H}$ is the Hamiltonian of the system;

$\mathbf{M}$ is the dimension of the corner-space;

$\mathbf{C}_i$ are the dissipators, with the specification of type and site index (i).

**Data:**

$\mathbf{n}_B$ is the number of blocks.

```
for i = 0 → n_s do
    push site with index i in the block
    while n_B ≠ 1 do
        for i = 0 → n_B do
            if i%4 = 0 then
                merge the blocks B[i] and B[i+1] putting B[i] spatially on the left
            else
                merge the blocks B[i] and B[i+1] putting B[i] spatially on the
                 right
            end if
            express the density matrix of the merged block in terms of an
             orthonormal basis
            if there is degeneration among eigenvalues then
                apply Gram-Schmidt orthonormalization process
            else
                use the basis formed by the eigenvectors of the density matrix
            end if
            get the pseudo-orthogonal matrix formed by the M most probable
             product states
            change of basis through this pseudo-orthogonal matrix
            get the density matrix in the corner-space
            calculate the expectation values of observables
            the (new) merged blocks replace the old ones
        end for
    end while
end for
```

# Appendix B

# Convergence and Errors

Before we examine the results obtained from the numerical methods, in this section a brief discussion on the convergence of the data, error calculus and the choice of parameters is done.

### B.0.1 Quantum Trajectories Method

The QT method, explained in section 3.1, doing the stochastic unraveling of the master equation, builds the quantum trajectories after which it is named. Every quantum trajectory corresponds to a simulated experiment and for the model under consideration, has an oscillatory profile as that displayed in fig. B.1. In order to stabilize the solution, for every quantum trajectory, the average in time is considered, starting from the end of the transient (needed for a solution of the Lindblad equation to converge into the stationary one).

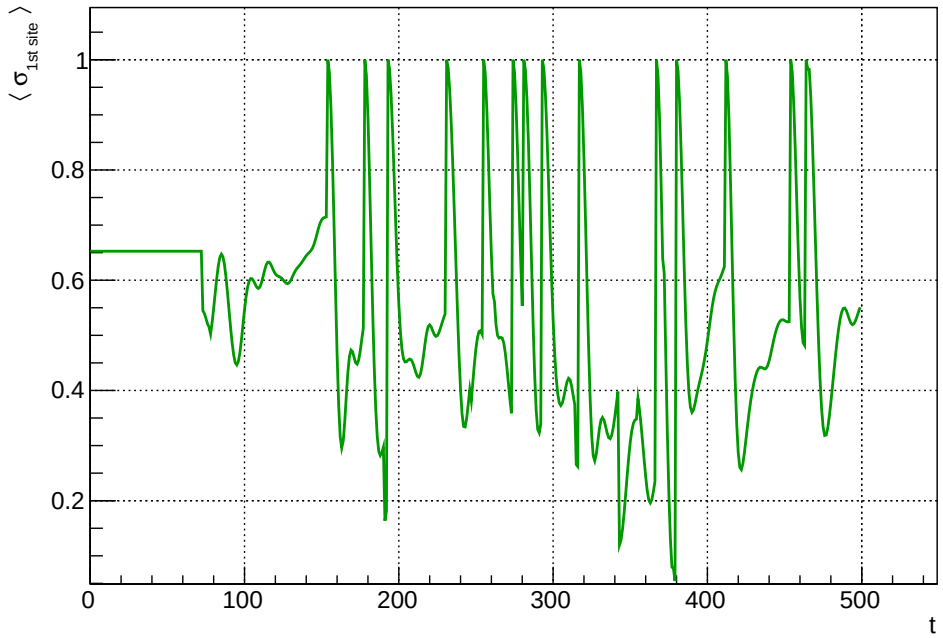


FIGURE B.1: Example of quantum trajectory; in particular, this is the expectation value of the magnetization of the first site of the chain, for $J_z = 1.1$ and $\gamma = 1$. The total elapsed time is $T = 500$, while the time step $dt = 0.1$.

For the same case considered in fig. B.1, the convergence of the mean values is shown in fig. B.2.

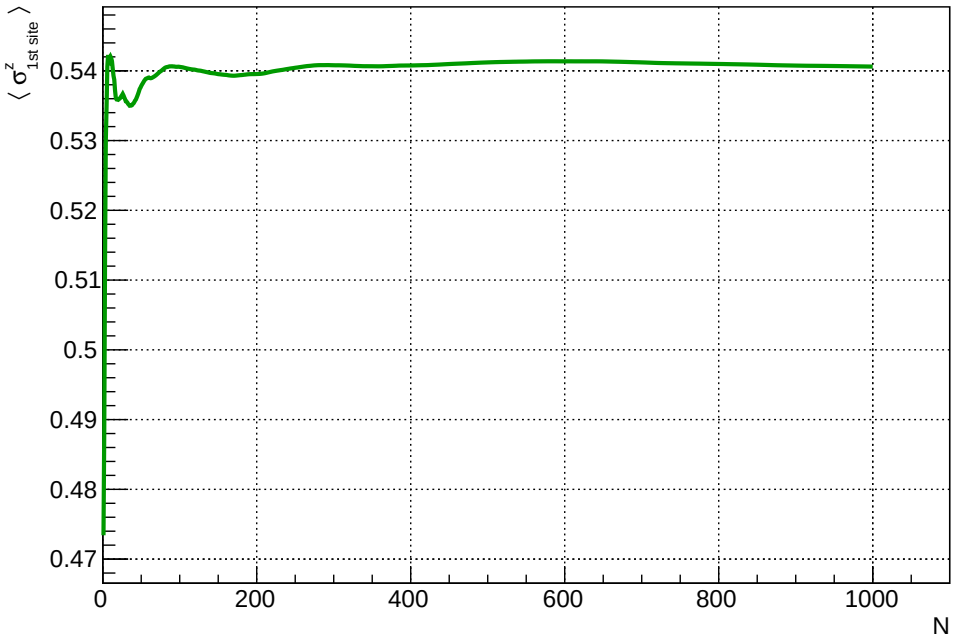


FIGURE B.2: Study of the convergence of the mean values of the quantum trajectories. For the case under consideration the number of events is $N = 1000$.

The study of the 8-sites chain was done with an elapsed time for every event of $T = 500$ and time-step $dt = 0.1$. The total number of simulated experiment is $N = 1000$.

As an error has been consider the standard deviation of the mean, i.e.

$$\sigma_{\text{mean}} = \frac{\sigma}{\sqrt{N}},$$

where $\sigma$ is the standard deviation of the mean in time in the quantum trajectory.

### B.0.2 Matrix Product Density Operators Method

The convergence of MPO method depends essentially on the setting of two parameters: the bond dimension and the number of Trotter steps. The fig. B.3 shows the convergence profile for a 8-sites chain for $J_z = 1$ and $\gamma = 1$. The same quantity can reach convergence in different times if, for example, $J_z$ assumes another value.

In the present work, for 8-sites chain it was considered a bond dimension $m = 100$ and Trotter steps in the range $[1200, 1500]$; for 12-sites chain was considered a bond dimension $m = 60$ and Trotter steps in the range $[1000, 2000]$; for 16-sites chain was considered a bond dimension $m = 80, 100$ and Trotter steps in the range $[1000, 1500]$.

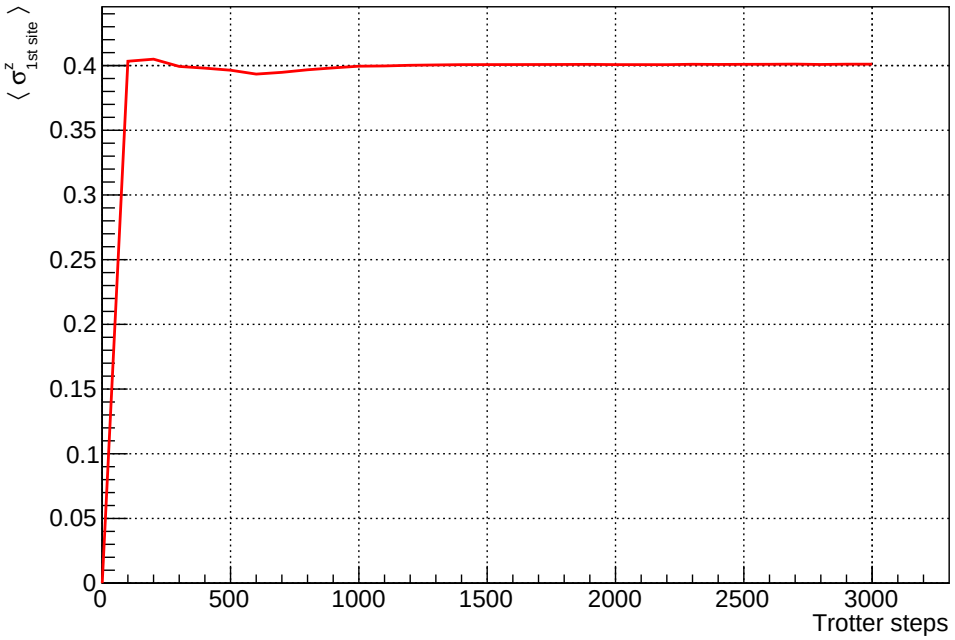


FIGURE B.3: Study of convergence of the MPO method for a 8-sites chain, for bond dimension m = 100 and T = 3000.

# Bibliography


[1] Luigi Amico et al. "Entanglement in many-body systems". In: *Rev. Mod. Phys.* 80 (2 May 2008), pp. 517–576. DOI: 10.1103/RevModPhys.80.517. URL: https://link.aps.org/doi/10.1103/RevModPhys.80.517.

[2] Dimitris G. Angelakis, Marcelo Franca Santos, and Sougato Bose. "Photon-blockade-induced Mott transitions and *XY* spin models in coupled cavity arrays". In: *Phys. Rev. A* 76 (3 Sept. 2007), p. 031805. DOI: 10.1103/PhysRevA.76.031805. URL: https://link.aps.org/doi/10.1103/PhysRevA.76.031805.

[3] G Benenti et al. "Charge and spin transport in strongly correlated one-dimensional quantum systems driven far from equilibrium". In: *Physical Review B* 80 (Jan. 2009). DOI: 10.1103/PhysRevB.80.035110.

[4] Karl Blum. *Density Matrix Theory and Applications*. Springer-Verlag Berlin Heidelberg, 2012.

[5] B.H. Bransden and C.J. Joachain. *Quantum Mechanics*. Pearson Education Limited, 2000.

[6] Heinz-Peter Breuer and Francesco Petruccione. *The Theory of Open Quantum Systems*. Oxford University Press, 2003.

[7] Rene Brun and Fons Rademakers. "ROOT - An Object Oriented Data Analysis Framework". In: *Nucl. Inst. Meth. in Phys. Res. A 389 (1997) 81-86* (Sept. 1996). DOI: http://root.cern.ch/.

[8] Gabriel G. Carlo et al. "Simulating noisy quantum protocols with quantum trajectories". In: *Phys. Rev. A* 69 (6 June 2004), p. 062317. DOI: 10.1103/PhysRevA.69.062317. URL: https://link.aps.org/doi/10.1103/PhysRevA.69.062317.

[9] Iacopo Carusotto and Cristiano Ciuti. "Quantum fluids of light". In: *Rev. Mod. Phys.* 85 (1 Feb. 2013), pp. 299–366. DOI: 10.1103/RevModPhys.85.299. URL: https://link.aps.org/doi/10.1103/RevModPhys.85.299.

[10] J Ignacio Cirac and Frank Verstraete. "Renormalization and tensor product states in spin chains and lattices". In: *Journal of Physics A: Mathematical and Theoretical* 42.50 (Dec. 2009), p. 504004. DOI: 10.1088/1751-8113/42/50/504004. URL: https://doi.org/10.1088%2F1751-8113%2F42%2F50%2F504004.

[11] Jean Dalibard, Yvan Castin, and Klaus Mølmer. "Wave-function approach to dissipative processes in quantum optics". In: *Phys. Rev. Lett.* 68 (5 Feb. 1992), pp. 580–583. DOI: 10.1103/PhysRevLett.68.580. URL: https://link.aps.org/doi/10.1103/PhysRevLett.68.580.

[12] S. Diehl et al. "Quantum states and phases in driven open quantum systems with cold atoms". In: *Nature Physics* 4 (Sept. 2008). DOI: 10.1038/nphys1073. URL: https://doi.org/10.1038/nphys1073.

[13] Rosario Fazio and Herre van der Zant. "Quantum phase transitions and vortex dynamics in superconducting networks". In: *Physics Reports* 355.4 (2001), pp. 235–334. ISSN: 0370-1573. DOI: https://doi.org/10.1016/S0370-1573(01)00022-9. URL: http://www.sciencedirect.com/science/article/pii/S0370157301000229.

[14] S. Finazzi et al. "Corner-Space Renormalization Method for Driven-Dissipative Two-Dimensional Correlated Systems". In: *Phys. Rev. Lett.* 115 (8 Aug. 2015), p. 080604. DOI: 10.1103/PhysRevLett.115.080604. URL: https://link.aps.org/doi/10.1103/PhysRevLett.115.080604.

[15] Mattias Fitzpatrick et al. "Observation of a Dissipative Phase Transition in a One-Dimensional Circuit QED Lattice". In: *Phys. Rev. X* 7 (1 Feb. 2017), p. 011016. DOI: 10.1103/PhysRevX.7.011016. URL: https://link.aps.org/doi/10.1103/PhysRevX.7.011016.

[16] Markus et al. Greiner. "Quantum phase transition from a superfluid to a Mott insulator in a gas of ultracold atoms". In: *Nature* 415 (6867 Jan. 2002). DOI: 10.1038/415039a. URL: https://doi.org/10.1038/415039a.

[17] Markus Greiner and Simon Fölling. "Optical lattices". In: *Nature - online* 453 (June 2008). DOI: https://doi.org/10.1038/453736a.

[18] Michael J. Hartmann, Fernando G. S. L. Brandão, and Martin B. Plenio. "Effective Spin Systems in Coupled Microcavities". In: *Phys. Rev. Lett.* 99 (16 Oct. 2007), p. 160501. DOI: 10.1103/PhysRevLett.99.160501. URL: https://link.aps.org/doi/10.1103/PhysRevLett.99.160501.

[19] Andrew A. Houck, Hakan E. Türeci, and Jens Koch. "On-chip quantum simulation with superconducting circuits". In: *Nature Physics* 8 (Apr. 2012). DOI: 10.1038/nphys2251. URL: https://doi.org/10.1038/nphys2251.

[20] Andrew A. Houck, Hakan E. Türeci, and Jens Koch. "On-chip quantum simulation with superconducting circuits". In: *Nature Physics* 8 (Apr. 2012). DOI: DOI:10.1038/NPHYS2251. URL: http://ee.princeton.edu/research/tureci/sites/default/files/nphys2251_0.pdf.

[21] A. Imamo lu et al. "Strongly Interacting Photons in a Nonlinear Cavity". In: *Phys. Rev. Lett.* 79 (8 Aug. 1997), pp. 1467–1470. DOI: 10.1103/PhysRevLett.79.1467. URL: https://link.aps.org/doi/10.1103/PhysRevLett.79.1467.

[22] University of Cologne - Institute for Theoretical Physics. URL: http://www.thp.uni-koeln.de/diehl/research.html.

[23] Jiasen Jin et al. "Cluster Mean-Field Approach to the Steady-State Phase Diagram of Dissipative Spin Systems". In: *Phys. Rev. X* 6 (3 July 2016), p. 031011. DOI: 10.1103/PhysRevX.6.031011. URL: https://link.aps.org/doi/10.1103/PhysRevX.6.031011.

[24] M.W. et al. Johnson. "Quantum annealing with manufactured spins". In: *Nature* 473 (May 2011). DOI: https://doi.org/10.1038/nature10012.

[25] Tony E. Lee, Sarang Gopalakrishnan, and Mikhail D. Lukin. "Unconventional Magnetism via Optical Pumping of Interacting Spin Systems". In: *Phys. Rev. Lett.* 110 (25 June 2013), p. 257204. DOI: 10.1103/PhysRevLett.110.257204. URL: https://link.aps.org/doi/10.1103/PhysRevLett.110.257204.

[26] Tony E. Lee, H. Häffner, and M. C. Cross. "Antiferromagnetic phase transition in a nonequilibrium lattice of Rydberg atoms". In: *Phys. Rev. A* 84 (3 Sept. 2011), p. 031402. DOI: 10.1103/PhysRevA.84.031402. URL: https://link.aps.org/doi/10.1103/PhysRevA.84.031402.

[27] Florence LENS laboratory. URL: http://www.lens.unifi.it/?include=research/dynamic_research&researcharea=Atomic%5C%20physics&active=research&menu=research/atomic_physics/atomic_physics_menu.

[28] Maciej Lewenstein et al. "Ultracold atomic gases in optical lattices: mimicking condensed matter physics and beyond". In: *Advances in Physics* 56.2 (2007), pp. 243–379. DOI: 10.1080/00018730701223200. eprint: https://doi.org/10.1080/00018730701223200. URL: https://doi.org/10.1080/00018730701223200.

[29] Andy C. Y. Li, F. Petruccione, and Jens Koch. "Resummation for Nonequilibrium Perturbation Theory and Application to Open Quantum Lattices". In: *Phys. Rev. X* 6 (2 June 2016), p. 021037. DOI: 10.1103/PhysRevX.6.021037. URL: https://link.aps.org/doi/10.1103/PhysRevX.6.021037.

[30] P. Li, Y. Gu, and Q. et al. Gong. "Generation of Ising interaction and cluster states in a one-dimensional coupled resonator waveguide". In: *Eur. Phys. J. D* 55 (2009). DOI: https://doi.org/10.1140/epjd/e2009-00188-3.

[31] Max Ludwig and Florian Marquardt. "Quantum Many-Body Dynamics in Optomechanical Arrays". In: *Phys. Rev. Lett.* 111 (7 Aug. 2013), p. 073603. DOI: 10.1103/PhysRevLett.111.073603. URL: https://link.aps.org/doi/10.1103/PhysRevLett.111.073603.

[32] Fabrizio Minganti et al. "Specrtal Theory of Liouvillians for Dissipative Phase Transitions". In: *arXiv:1804.11293 [quant-ph]* (May 2018).

[33] Klaus Mølmer, Yvan Castin, and Jean Dalibard. "Monte Carlo wave-function method in quantum optics". In: *J. Opt. Soc. Am. B* 10.3 (Mar. 1993), pp. 524–538. DOI: 10.1364/JOSAB.10.000524. URL: http://josab.osa.org/abstract.cfm?URI=josab-10-3-524.

[34] Michael A. Nielsen and Isaac L. Chuang. *Quantum Computation and Quantum Information*. Cambridge University Press, 2000.

[35] Changsuk Noh and Dimitris G Angelakis. "Quantum simulations and many-body physics with light". In: *Reports on Progress in Physics* 80.1 (Nov. 2016), p. 016401. DOI: 10.1088/0034-4885/80/1/016401. URL: https://doi.org/10.1088%2F0034-4885%2F80%2F1%2F016401.

[36] John Preskill. *Quantum Information*. Lecture Notes. California Institute of Technology, July 2015.

[37] Toma ž Prosen. "Exact Nonequilibrium Steady State of a Strongly Driven Open $XXZ$ Chain". In: *Phys. Rev. Lett.* 107 (13 Sept. 2011), p. 137201. DOI: 10.1103/PhysRevLett.107.137201. URL: https://link.aps.org/doi/10.1103/PhysRevLett.107.137201.

[38] Tomaž Prosen. "Third quantization: a general method to solve master equations for quadratic open Fermi systems". In: *New Journal of Physics* 10.4 (Apr. 2008), p. 043026. DOI: 10.1088/1367-2630/10/4/043026. URL: https://doi.org/10.1088%2F1367-2630%2F10%2F4%2F043026.

[39] Tomaž Prosen and Marko Žnidarič. "Matrix product simulations of non-equilibrium steady states of quantum spin chains". In: *Journal of Statistical Mechanics: Theory and Experiment* 2009.02 (Feb. 2009), P02035. DOI: 10.1088/1742-5468/2009/02/p02035. URL: https://doi.org/10.1088.

[40] Juris Reisons, Eduardo Mascarenhas, and Vincenzo Savona. "Emergent transport in a many-body open system driven by interacting quantum baths". In: *Physical Review B* 96 (June 2017). DOI: 10.1103/PhysRevB.96.165137.

[41] D. Rossini. URL: https://daviderossini.wordpress.com/courses/.

[42] Peter Štelmachovi č and Vladimır Bu žek. "Dynamics of open quantum systems initially entangled with environment: Beyond the Kraus representation". In: *Phys. Rev. A* 64 (6 Nov. 2001), p. 062106. DOI: 10.1103/PhysRevA.64.062106. URL: https://link.aps.org/doi/10.1103/PhysRevA.64.062106.

[43] Conrad Sanderson and Ryan Curtin. "A User-Friendly Hybrid Sparse Matrix Class in C++". In: *Lecture Notes in Computer Science (LNCS)*. Vol. 10931. 2018, pp. 422–430.

[44] Conrad Sanderson and Ryan Curtin. "Armadillo: a template-based C++ library for linear algebra". In: *Journal of Open Source Software* 1 (2016), p. 26.

[45] U. Schollwöck. "The density-matrix renormalization group". In: *Rev. Mod. Phys.* 77 (1 Apr. 2005), pp. 259–315. DOI: 10.1103/RevModPhys.77.259. URL: https://link.aps.org/doi/10.1103/RevModPhys.77.259.

[46] Ulrich Schollwöck. "The density-matrix renormalization group in the age of matrix product states". In: *Annals of Physics* 326.1 (2011). January 2011 Special Issue, pp. 96–192. ISSN: 0003-4916. DOI: https://doi.org/10.1016/j.aop.2010.09.012. URL: http://www.sciencedirect.com/science/article/pii/S0003491610001752.

[47] C. Schweizer et al. "Spin Pumping and Measurement of Spin Currents in Optical Superlattices". In: *Phys. Rev. Lett.* 117 (17 Oct. 2016), p. 170405. DOI: 10.1103/PhysRevLett.117.170405. URL: https://link.aps.org/doi/10.1103/PhysRevLett.117.170405.

[48] Bruce W. Shore and Peter L. Knight. "The Jaynes-Cummings Model". In: *Journal of Modern Optics* 40.7 (1993), pp. 1195–1238. DOI: 10.1080/09500349314551321. eprint: https://doi.org/10.1080/09500349314551321. URL: https://doi.org/10.1080/09500349314551321.

[49] A. Tomadin and Rosario Fazio. "Many-body phenomena in QED-cavity arrays (Invited)". In: *J. Opt. Soc. Am. B* 27.6 (June 2010), A130–A136. DOI: 10.1364/JOSAB.27.00A130. URL: http://josab.osa.org/abstract.cfm?URI=josab-27-6-A130.

[50] F. Verstraete, J. J. Garcıa-Ripoll, and J. I. Cirac. "Matrix Product Density Operators: Simulation of Finite-Temperature and Dissipative Systems". In: *Phys. Rev. Lett.* 93 (20 Nov. 2004), p. 207204. DOI: 10.1103/PhysRevLett.93.207204. URL: https://link.aps.org/doi/10.1103/PhysRevLett.93.207204.

[51] Guifré Vidal. "Efficient Classical Simulation of Slightly Entangled Quantum Computations". In: *Phys. Rev. Lett.* 91 (14 Oct. 2003), p. 147902. DOI: 10.1103/PhysRevLett.91.147902. URL: https://link.aps.org/doi/10.1103/PhysRevLett.91.147902.

[52] Guifré Vidal. "Efficient Simulation of One-Dimensional Quantum Many-Body Systems". In: *Phys. Rev. Lett.* 93 (4 July 2004), p. 040502. DOI: 10.1103/PhysRevLett.93.040502. URL: https://link.aps.org/doi/10.1103/PhysRevLett.93.040502.

[53] Steven R. White. "Density Matrix Formulation for Quantum Renormalization Groups". In: *Physical Review Letters* 69.19 (Nov. 1992).

[54] Steven R. White. "Density-matrix algorithms for quantum renormalization groups". In: *Phys. Rev. B* 48 (14 Oct. 1993), pp. 10345–10356. DOI: 10.1103/PhysRevB.48.10345. URL: https://link.aps.org/doi/10.1103/PhysRevB.48.10345.

[55] Kenneth G. Wilson. "The renormalization group: Critical phenomena and the Kondo problem". In: *Rev. Mod. Phys.* 47 (4 Oct. 1975), pp. 773–840. DOI: 10.1103/RevModPhys.47.773. URL: https://link.aps.org/doi/10.1103/RevModPhys.47.773.

[56] Marko Žnidari č. "Spin Transport in a One-Dimensional Anisotropic Heisenberg Model". In: *Phys. Rev. Lett.* 106 (22 May 2011), p. 220601. DOI: 10.1103/PhysRevLett.106.220601. URL: https://link.aps.org/doi/10.1103/PhysRevLett.106.220601.

[57] W. Zheng. *Series Expansion Methods for Strongly Interacting Lattice Models*. Cambridge University Press, 2006.

[58] Michael Zwolak and Guifré Vidal. "Mixed-State Dynamics in One-Dimensional Quantum Lattice Systems: A Time-Dependent Superoperator Renormalization Algorithm". In: *Phys. Rev. Lett.* 93 (20 Nov. 2004), p. 207205. DOI: 10.1103/PhysRevLett.93.207205. URL: https://link.aps.org/doi/10.1103/PhysRevLett.93.207205.